UCRL-20031

MASTER

THE BRANCHING RATIO $K \rightarrow e\nu/K \rightarrow \mu\nu$: A TEST OF V-A THEORY OF WEAK INTERACTIONS

John Frederick McReynolds
(Ph. D. Thesis)

September 16, 1970

AEC Contract No. W-7405-eng-48

LAWRENCE RADIATION LABORATORY
UNIVERSITY of CALIFORNIA BERKELEY

UCRL-20031

DISCLAIMER

THIS PAGE

WAS INTENTIONALLY

LEFT BLANK

THE BRANCHING RATIO $K \to e\nu/K \to \mu\nu$: A TEST OF V–A THEORY OF WEAK INTERACTIONS

Contents

THE BRANCHING RATIO $K \to e\nu/K \to \mu\nu$: A TEST OF V–A THEORY OF WEAK INTERACTIONS

John Frederick McReynolds

Lawrence Radiation Laboratory
University of California
Berkeley, California

September 16, 1970

ABSTRACT

An optical spark chamber experiment utilizing an axially focusing cylindrically symmetric spectrometer has gathered 62.6 ± 11 $K \to e\nu$ events, giving a branching ratio Ke_2 $K\mu_2 = 2.32 \pm .39 \times 10^{-5}$, and setting new limits of

$$0 \leq \left| \frac{f_P}{f_A} \right| < 1.75 \times 10^{-4} \quad \text{or} \quad 1.82 \times 10^{-3} < \left| \frac{f_P}{f_A} \right| < 2.12 \times 10^{-3}$$

A beam of 500 K^+/pulse with $K^+/\pi^+ = .002$ from the Bevatron External Proton Beam was stopped on the spectrometer axis. Charged particles over .4 of 4π were allowed a single orbit in the spectrometer. Such particles in a 12% momentum bite passed through a 300 psi ethane Cherenkov counter, a scintillator and spark chamber array designed for ± 1% momentum analysis, and into a lead cylinder, spark chamber, and scintillator array designed for muon rejection.

Events were scanned and measured on SASS, an automatic scanning system. A total of 150,000 events were measured, analyzed, and kinematically reconstructed. These events satisfied trigger requirements for Ke_2, for $K \to$ charged particle + γ, and for normalization to $K\mu_2$, $K\pi_2$, and Ke_3.

UCRL-20031

I. INTRODUCTION

The Vector–Axial Vector (V–A) theory has had wide success in predicting results of weak interactions, in measurements of decay parameters of various particles into lighter particles and in μ and e capture by nuclei. Such experiments cover nuclear β–decay and all of the long–lived elementary particle decays (e.g., μ, π, K, n, Λ, Σ).

While V–A has in general predicted the observed decay rates, the possibility of a large admixture of pseudo scalar, scalar, and tensor (P, S, T) interactions cannot be ruled out without high–precision experiments. This experiment is a measurement of the pseudo scalar contamination. The companion experiment to Ke_2, the πe_2 has given a branching ratio of $(1.25 \pm .03) \times 10^{-4}$. If the interaction were pure A (there is no V, S, or T contribution in this interaction as the π is a pseudo scalar coupled to the "vacuum" of pure leptons), the branching ratio would be calculated to be 1.25×10^{-4}, while if the decay were pure P, the rate would be 3.5. This result indicates $f_P/(m_e f_A/m_\pi) = 0$ [or –2, as f_P and f_A enter the decay rate as $(f_P + \frac{m_e}{m_\pi} f_A)^2$]. The purpose of this experiment is to test for changes in the interaction due to strangeness or due to a momentum–transfer dependence in f_P [if $f_P = f_P(q^2)$, perhaps $f_P(m_\pi^2) \neq f_P(m_K^2)$]. The V–A prediction for the branching ratio $(K \to e\nu)/(K \to \mu\nu)$ is 2.22×10^{-5}, including radiative corrections.

Two other groups[1,2] have performed ke_2 searches as addenda to $K \to \pi^o e\nu$ experiments, with a total of 17 ± 7 events. This experiment was planned to pick up 500 to 1000 such events, requiring a spectrometer of wide angular acceptance, as a beam of 1000 stopping K^+/pulse in a 7 gm/cm^2 range bite was the maximum available.

The experiment was performed at the Bevatron at the Lawrence Radiation Laboratory in Berkeley between the dates September 10, 1967 through June 10, 1968. A total of 100 12-hour periods were used.

II. THEORY

A. $K \to e\nu$ (without electromagnetic effects)

The general form of the interaction $M \to \ell\nu$[3] (meson → lepton + neutrino) according to the current–current theory of weak interactions is

$$< \ell\nu \mid H_w \mid M > = \sum_i C_i < \ell\nu \mid \Gamma^i \mid \psi > < \psi \mid \Gamma^i \mid M >$$

where H_w is the complete weak Hamiltonian, the i = S, P, V, A, T, the C_i reflecting the strengths of interaction, the Γ^i the particular form of interaction, and $\mid \psi > < \psi \mid$ is the sum over intermediate states. Possible states are $\mid p\,\bar{\Lambda} >$ or $\mid \bar{n}\,\Sigma^+ >$.

As noted before, only P and A are consistent with parity and angular momentum conservation for M, a pseudoscalar spin–zero meson. A is an axial vector interaction, hence must be coupled to the only vector available, the momentum transfer to the lepton pair, $q^\mu = q_e^\mu + q_\nu^\mu$, normalized to the meson mass, and a function of the meson mass. By Lorentz invariance its form is

$$C_A < \psi \mid \Gamma^A \mid M > = i \frac{q^\mu}{m_M} f_A (m_M^2) \times (2\pi)^{3/2}$$

m_M is chosen to make f_A dimensionless and to introduce no "new" numbers, as

$$\frac{q^\mu}{m_M} \cdot \frac{q^\mu}{m_M} = \frac{m_M^2}{m_M^2} = 1$$

P, a pseudoscalar, is only a function of the meson mass.

$$C_P < \psi \mid \Gamma^A \mid M > = i f_P (m_M^2) \times (2\pi)^{3/2}$$

The lepton currents are

$$< \ell\nu \mid \Gamma^P \mid \psi > = U(P_e)\ \gamma^5\ \bar{V}\ (P_\nu)\ \sqrt{2m_\nu}/(2\pi)^3$$

$$< \ell\nu \mid \Gamma^A \mid \psi > = U(P_e)\ \gamma^\mu\ \gamma^5\ \bar{V}\ (P_\nu)\ \sqrt{2m_\nu}/(2\pi)^3$$

Using the Dirac equation, $(q_\ell^\mu\ \gamma^\mu + m_\ell)\mid \ell > = 0$ and $q_\nu^\mu\ \gamma^\mu \mid \nu > = 0$, which causes the m_ℓ factor multiplying f_A, the decay rate can be easily calculated

$$\Gamma\ (M \to \ell\nu) = \frac{m_M}{8\pi} \left(\frac{m_M^2 - m_\ell^2}{m_M^2}\right)^2 \left(\frac{m_\ell}{m_M}\ f_\Lambda + f_P\right)^2$$

For the π meson

$$R = \frac{\Gamma(\pi \to e\nu)}{\Gamma(\pi \to \mu\nu)} = \left(\frac{m_\pi^2 - m_e^2}{m_\pi^2 - m_\mu^2}\right)^2 \frac{\left(\frac{m_e}{m_\pi}\ f_A + f_P\right)^2}{\left(\frac{m_\mu}{m_\pi}\ f_A + f_P\right)^2}$$

Thus

$$R_\pi\ (\text{pure A}) = 1.25 \times 10^{-4}$$

$$R_\pi\ (\text{pure P}) = 3.5$$

For the case that both A and P are non-zero, R can go as low as zero (with $f_P/\left(\frac{m_e}{m_\pi}\ f_A\right) = -1$) and as high as the pure P ratio.

In K decay the situation is slightly different as C_A and C_P are reduced by the Cabibbo factor,[4] which applies equally to Ke_2 or $K\mu_2$. Thus, assuming lepton universality in K and π decays, the formula for R_K should be the same as for the pion, changed only by the meson mass.

$$\frac{\Gamma(K \to e\nu)}{\Gamma(K \to \mu\nu)} = R_K = \left(\frac{m_K^2 - m_e^2}{m_K^2 - m_\mu^2}\right)^2 \left(\frac{\frac{m_e}{m_K}\ f_A + f_P}{\frac{m_\mu}{m_K}\ f_A + f_P}\right)^2$$

R (pure A) = 2.58×10^{-5}

R (pure P) = 1.10

B. Electromagnetic Corrections[5,6,7]

The relative decay rates are changed due to exchange of virtual photons, which changes the mass of the lepton, and the emission of real photons of low enough energy that the decay secondary remains within the experimental momentum resolution.

The renormalization due to virtual photons is actually a statement that the weak interaction operates on lepton "bare" masses. This results in a factor, calculable from quantum electrodynamics (to order α), of

$$1 + \delta = \left(\frac{m_e / m_{e_o}}{m_\mu / m_{\mu_o}} \right)^2 = 1 - \frac{3\alpha}{\pi} \ln \frac{m_\mu}{m_e} = .963$$

Undetected inner bremsstrahlung and corrections to the decay operator due to virtual photon emission and re–absorption must be calculated together to preserve gauge invariance. This process leads to a factor $f = \dfrac{1 + \eta_e + \beta_e}{1 + \eta_\mu + \beta_\mu}$ where[6]

$$\eta_\ell = \frac{\alpha}{\pi} \left[\frac{3}{2} \ln \frac{2\Delta E}{m_K} + b(X) \ln (1 - X^2) + \frac{X^2(8 - 5X^2)}{2(1 - X^2)} \ln X \right.$$

$$\left. + \frac{2(1 + X^2)}{1 - X^2} L(1 - X^2) + \frac{19 - 25X^2}{8(1 - X^2)} \right]$$

ΔE = maximum acceptable energy loss

$$X = \frac{m_\ell}{m_K}$$

$$b(X) = \frac{1 + X^2}{1 - X^2} \ell n\ X$$

and

$$L(y) = \int_0^y \frac{\ell n\ (1 - t)}{t}\ dt = -\sum_{K=1}^{\infty} \frac{y^K}{K^2}$$

η_ℓ = virtual photon correction for lepton ℓ

β_e = inner bremsstrahlung correction for lepton ℓ

$$\beta_e = \frac{\alpha}{\pi}\left[-b(X)\left(\ell n\ \left(\frac{m_K}{2\Delta E}\right) + 2\ \ell n\ (1 - X^2) - \frac{3}{4}\right)\right.$$

$$\left. - \frac{X^2\ (10 - 7\ X^2)}{2\ (1 - X^2)^2}\ \ell n\ X + \frac{2\ (1 + X^2)}{1 - X^2}\ L\ (1 - X^2) + \frac{15 - 21\ X^2}{8\ (1 - X^2)}\right]$$

$\eta_e = -\ .0340$

$\eta_\mu = -\ .0056$

$\beta_e = -\ .0850$

$\beta_\mu = -\ .0079$

$$f = \frac{.881}{.987} = .893$$

The entire correction is then

$$C_\gamma = f\ x\ (1 + \delta) = .861$$

These calculations do not include a structure effect (see Section V.A.4).

The theoretical ratio is then

$$R_{TH} = \frac{\Gamma(K \to e\nu)}{\Gamma(K \to \mu\nu)} = R_K \; C_\gamma = \begin{cases} 2.22 \times 10^{-5} & \text{(pure A)} \\ .948 & \text{(pure P)} \end{cases}$$

III. EXPERIMENTAL APPARATUS

A. The Stopping K^+ Beam

Beam 5b of the external proton beam (see Fig. 1), Channel 1, was used with a uranium target to produce 540 MeV/c ± 2% secondaries at 0°. These secondaries were bent from the EPB by a C-magnet directly behind the target, passed through a quadrupole doublet, a 500 KV, 10 ft. electrostatic separator, a second bending magnet, and were focused by the second quadrupole doublet onto the collimator at the first focus. Approximately 3 inches after this focus were placed a 1/8" scintillator (S1) and a differential Cherenkov counter (C_π), designed to count π mesons but not K's. The beam then passed through the third quadrupole set, the third bending magnet and the fourth quadrupole doublet, which focused and recombined the beam on the degrader and stopper within the M5 magnet.

One-half inch before the degrader (11" beryllium) was placed a 1/2 thick scintillator (S2), and directly after the degrader, a 1/4" x 1" x 1" scintillator (S3). Beam particles then passed through a 4 x 1/8" gap x 1-1/8" x 1-1/8" spark chamber and into the stopper, a polyethylene cylinder 2-1/2" length, 1-1/4" diameter (see Fig. 2).

The S1 and S2 photomultipliers were plateaued on K's. These counters were equally efficient in counting π's or K's, which have approximately equal scintillation pulses at 500 MeV/c. However, as the two counters were separated by approximately 16 feet, π's arrived at S2 some 5 nanoseconds before K's, and could be discriminated against by timing by a factor of 5:1. The S3 discriminator was set for the larger pulses emitted by slower K mesons (30 to 200 MeV/c). (The momentum spread into the

degrader was 530 to 550 MeV/c.) This allowed another discrimination by about 4:1. In addition the beam Cherenkov counter C_π was used in anti–coincidence, for another factor of 5:1. The total π rate in the beam was monitored by $S1_\pi$ S2 (timed for π's). The $\frac{\pi}{K}$ ratio was 50:1, giving BK a 30% π contamination. (BK = $S1_K$ S2 $S3_K$ $\overline{C}_\pi$, $S1_K$ = S1 timed for K's, $S3_K$ = S3 signal discriminated by pulse height for K's.)

The stopper, a polyethylene cylinder 2–1/2" long, 1–1/4" diameter, was enclosed in a 1/8" thick 3" long cylindrical scintillator S4, to record the charged decay secondary of a stopping particle. S4 was timed with respect to BK with S2 timing, requiring the signal to be at least 10 nanoseconds after the BK signal (about one K lifetime) and not more than 70 ns. after BK. The delay between S4 and BK was recorded by a time–to–amplitude converter and a 100–channel pulse height analyzer. Large pulses from S4 were set in prompt anti–coincidence to DK, to throw out any π which passed lengthwise through the counter. An updating gate (Mi) prevented recording any particle which entered the system less than 100 ns. after another beam particle.

The absolute monitor of the K rate was then DKM = (BK) ($S4_{\text{delayed}}$) ($\overline{\text{Mi}}$)($\overline{S4}_{\text{large}}$). There was no π contamination in DKM.

B. The M–5 Spectrometer

The general design of this spectrometer has been described.[8] Our basic requirements were a large aperture, a possibility of measuring momenta up to 260 MeV/c with ± 1% accuracy, a possibility of analyzing charged secondaries in a variety of ways, and a relatively low background. The spectrometer, similar to one first described by Richardson for studying β decay, was an axially symmetric, axially focusing magnet

(see Figs. 2, 3). Particles starting on the axis and on the central plane (plane of symmetry) are focused back to that, while particles starting on axis but off the median plane are focused to a region on the axis an equal distance on the opposite side of the median plane, quite analogous to the focusing of a spherical mirror.

In general, only one momentum and starting point can be focused back to an exact point, in accordance with Liouville's theorem. Momenta and starting points in the region of the "object" or first focal point are returned to the region of the "image" or second focal point with some chromatic (momentum-dependent) and spherical aberrations. These aberrations are most independent and must be traded off against each other to obtain an acceptable field shape.

For the purpose of this experiment, a relatively narrow momentum spread with maximum aperture was needed, as the decay secondaries of most interest, $K \rightarrow e\nu$, $K \rightarrow \mu\nu$, and $K \rightarrow \pi\pi$ each have a unique momentum. For electron calibration purposes, the peak of the $K \rightarrow \pi e\nu$ electron spectrum at 150 MeV was used. The M-5 magnet at full power could produce the field needed to capture particles starting on axis with up to 270 MeV/c with a maximum orbit radius of 35 inches. With a field of 18,600 gauss on the axis, tapering to 15,800 at 35 inches (see Fig. 4) in the median plane, Ke_2 secondaries at 247 MeV/c were captured and focussed.

The M-5 pole tips and current settings were designed by trial and error, starting with the ellipsoidal field which was known to give best focusing for an on-axis and central plane particle of specific momentum. An ellipsoidal field is produced by hyperboloidal iron pole tips without saturation. The cases including saturation were computer-simulated using

CTRIM, a program for solving cylindrically symmetric boundary-value problems.[9] Orbits were stepwise integrated in the generated test fields using the ORBIT-ARKINT-FUNCT particle orbit program[10] to find a first guess for currents in the magnet coils. The magnet was measured at 40 different field values and orbits again shot to determine optimum operating conditions. The CTRIM calculated fields differed from the measurements at most by 3%, with an overall accuracy better than 1%. The magnet was remeasured at the end of the experiment. The field was fitted to spherical Legendre polynomials for smoothing, and the fitted field used in momentum analysis.

C. Orbit Identification

(See Figs. 2, 3, 20)

The stopper was centered on the axis of the beam, 5-1/2" downstream from the central plane. The stopper diameter of 1-1/4" resulted in a band 2" wide at the outer radius. From computer simulation of orbits a set of nine equally-spaced identical scimitar-shaped counters on the outer edge of the orbit was determined to be sufficient to provide an acceptance for momenta $\Delta P/P$ = 12% FWHM with all orbits within 2% of the central focused momentum having equal acceptance after folding in energy loss and stopper size. This effect resulted in equal acceptance for Ke_2 at Ke_2 magnet setting and for $K\mu_2$ at the $K\mu_2$ setting. The outer radius counters had inner edges at 28.75" spherical radius to give an equal lower momentum cut-off at all polar angles of emission of the secondaries. Particles in the momentum bite were accepted from .25 radians below to .50 above the median plane. The outer edge of the counters was 5.75" from the inner

edge on the central plane, with the same radius cut of 28.75", so that the spherical radial depth of the scintillators tapered to 4.75" at the extremities.

The light pipes for these counters (see Fig. 5) cannot be described in their full majesty and horror. Suffice it to say that light from the 1/4" scintillator had to pass through two 45° reflections, three bends, 5 to 9 feet of lucite, and 2 to 30 inches of Pilot B to get to its respective photo cathode. The 6810 RCA photomultipliers were placed on top and bottom of the magnet. The counters averaged 90% efficiency at 2300 volts (average). These complicated light pipes are another reflection of the problem of packing a large number of devices in a small and almost completely enclosed space. These light pipes came out of the magnet between the magnet coils, along with 18 other light pipes and 216 spark chamber cables.

The outer radius counter signals were put in triple coincidence with the proper two members of a set of eighteen stave inner (I) counters, each 1/8" x 30" x 2-1/4", taped together to form a 15" dia. barrel centered in the magnet. Stave outputs were discriminated and added in pairs to form an effective nine inner radius counters.

A typical orbit might pass through I1, at the start of the measured orbit, 03 in the middle, and I5 at the end. The particle precessed approximately 160° from I1 to I5, taking nine nanoseconds. Hence the "start" signal had to be delayed for proper timing. To check for negative particles orbitting, the orbit coincidence system could be "reversed" (e.g., I5 03 I1). The magnetic field was also reversed to check for asymmetries in the spectrometer.

D. Electron, Muon, and Gamma Identification

The stopper, enclosed in its scintillator S4, was supported inside an aluminum-walled 20 Atm. ethane gas Cherenkov counter, with a .080" spherical wall through which orbits exited (see Fig. 2). Light from electrons was reflected from a 2-cone aluminized mylar mirror to four RCA C-7046 5" photomultipliers behind 1" quartz windows at the downstream end of the magnet. The signals from the tubes were discriminated and added. The electron (E) trigger required signals from two tubes, with no tube having a signal greater than 5 times the normal electron signal. Large pulses came mainly from pions creating Cherenkov light in the quartz windows and knocking on electrons in the degrader.

Muons were not discriminated against in the triggering. Two devices were used for their identification in later analysis. At the end of the orbit, at which point the particles were focused to the upper half of the axis, a stainless steel cylinder filled with lead, 5.5" inside radius, 7.0" outside radius, 10" long, was placed with the downstream edge at the median plane (see Figs. 2, 3). This cylinder was six radiation lengths thick, so that electrons generally showered while passing through it, while muons were simply slowed and scattered, stopping in the opposite wall of the cylinder.

Within the lead cylinder was placed a 4 gap (3/8" gap) cylindrical spark chamber with the downstream edge at the median plane. Within this chamber was placed a 1/4" thick cylindrical scintillator (M), 7.5" outside diameter, with a light pipe curling out through the hole in the upstream face of the magnet, viewed by two photomultipliers. The signals were added, discriminated, coincidenced with the spark chamber trigger,

and displayed with a light on the data box.

To detect gamma rays a set of eighteen 3/4" x 12" x 24" counters were placed at 36" radius, behind 1/4" sheets of lead (1 radiation length). These counters surveyed approximately .3 of 4π solid angle. The counters were discriminated, coincidenced with the trigger, and displayed on the data box, as well as being added together amplified, and discriminated to form the gamma (G) trigger requirement. These counters were needed to study decays of the type $K \rightarrow e\nu\gamma$ in $K \rightarrow e\nu$, and provide a clean sample of $K \rightarrow \pi^o e\nu$ events, with $\pi^o \rightarrow \gamma\gamma$.

E. Fast Electronics and Triggering

(See Fig. 6)

As stated before, DKM = $(BK)(S4_{delayed})\ (M\bar{I})(S\bar{4}_{large})$. DKM was coincidenced with O and with either E or G to form KOE or KOG, which were the two trigger requirements for magnet settings Ke_2, $K\pi_2$, and Ke_3 (see Table 1). For $K\mu_2$ normalization runs KO was required for the trigger, achieved by switching E out of KOE.

Scalars monitored the outputs of MON, a three–fold scintillator coincidence, aimed at the EPB target, BEV, the number of Bevatron pulses per run, B_π, BK, DK, DKM, KO, KOE, KOG, the eighteen possible O signals, and the Cherenkov counter noise. The scalars were typed out after every run. Nominal run lengths are listed in Table 1 and scalar nomenclature in Table 6.

The discriminators of the O, I, and G counters were built at LRL and the O 18–fold coincidence was built by the Lofgren Group. All other fast discriminators and coincidence electronics were Chronetics (100 series).

F. Orbit Spark Chambers

Thin plate spark chambers were placed so that the momentum of the orbiting particle could be determined with high accuracy. The large cylindrical chamber showed tracks at the start and end of the orbit while the outer radius chambers (two beside each outer radius counter) showed tracks near the midpoint of the orbit. The large cylindrical chamber was placed outside the I-barrel of scintillators. It was 20" long, 4 gaps, each 1/2" wide, made of .005" aluminum cylinders, the innermost plate at 8.125" radius (see Figs. 2, 3). The chamber was supported at its upstream end and was quite rigid in its place. A 72-face 7° echelon mirror to measure depth in the chamber was placed at the downstream end of the chamber (see Fig. 20a). The downstream end track and reflection (outgoing) were therefore more closely spaced than the upstream (returning) track and reflection. The mirrors were each .85" x 2.2".

The outer radius chambers had two 3/8" gaps with foam plates covered with .001" foil and viewed through the inner radius edge (see Figs. 2, 3, 9). The outer, upstream, and downstream edges followed the contours of the outer radius counters, while the inner faces were flat 1/32" lucite at 24.5" cylindrical radius.

The large cylindrical chamber was pulsed at 14 kilovolts (KV), 16,000 picafarads (pf), each outer radius chamber 12 KV, 8000 pf., the small cylindrical chamber, 10 KV, 16,000 pf., the beam chamber 4 KV, 400 pf. The chambers were triggered by a 10 KV gap fired by a 1.5 KV thyratron. All gaps had an RC decay of 100 ns. The outer radius chambers needed a higher voltage due to line losses in the 25' input

cables (five 50 Ω cables in parallel per chamber).

The chambers were regularly monitored with Tektronix 519 oscilloscope as well as continuously monitored by an alarm system for slow or random pulses.

G. Slow Electronics, Camera, and Data Box

The data box (see Fig. 7) was a set of 64 xenon lights to display information on each frame of the film. Four circular lights at the outer edge of the data box were the master fiducials. The first row displayed the run and frame numbers as two 15–bit binary numbers. The first eighteen lights in the second row displayed the gamma counter information, a light on indicating that that gamma counter had recorded a pulse in coincidence with DKO timed to S4. The other twelve lights recorded the trigger type, KOE or KOG, the gas Cherenkov counter signal (E), the cylindrical muon counter (M), and the K lifetime (eight lights in binary–coded decimal).

The K lifetime was measured by a time–to–height converter turned on by BK and off by DKM timed to S4. This signal was input to a 100–channel pulse–height analyzer. The PHA signal was coded and displayed on the data box. The K lifetime measurement is valuable to check for backgrounds, which appear as prompt or flat distributions.

The system was gated off for 70 milliseconds after each trigger to allow the Flight Research 35 mm camera to advance. The film was Eastman Kodak 2498.

H. Optics

The inner radius optics, including the large cylindrical chamber, small cylindrical chamber, and beam chambers, was straightforward, using

all plane mirrors. The beam chamber was viewed through two 43° prisms mounted on its sides, through the hole in the M counter. The large cylindrical chamber stereo mirror, viewed through the large cylindrical chamber, has been described. The small cylindrical chamber, with no stereo mirror, was viewed along with the large cylindrical chamber through three large plane mirrors mounted on the upstream end of the magnet. The mirror in front of the optics hole in the magnet had a hole through which the beam passed. The large cylindrical chamber was viewed through a spherical lucite field lens mounted on the chamber.

Figucials for the cylindrical chambers were Xenon lamp lighted spots mounted on the lead cylinder. Beam chamber fiducials were flashlight bulbs mounted on the sides of the prisms.

The outer radius optics[11] (see Figs. 8, 9, A1) was essentially a nine-fold symmetric microscope looking at a dual fisheye. Each outer radius chamber pair had two 2-1/2" radius fisheye concave spherical mirrors, one mounted upstream, the other downstream, providing a stereo approximately 90° apart. The images of these two mirrors were collected by two mirrors mounted between the chamber pair, on the fiducial support, in the center plane of the magnet at 34" radius. The light went towards the axis and upstream to a flat mirror, through an achromatic lens and acutely upstream to the two large mirrors mounted on the front of the magnet around and below the beam, then to one of a ring of nine spherical 8" diameter, 62" focal length astronomical mirrors, thence to the camera.

The demagnification of the inner radius optics was 100:1. The demagnification of the outer radius optics tapered from 100:1 at the near-to-the-fisheye end to 300:1 at the far extreme of the chamber.

The outer radius fiducials were mounted on the magnet yoke, bolted to the upstream end and sliding on a bolt in a hole at the downstream end. This was necessary as the yoke flexed up to .050" at high fields. The fiducial panel was mounted at 34.8" in the center plane with a 32.5" radius on the face. Eight 1" circles were cut in the face, spaced at equal distances above and below the median plane, illuminated from the rear by electro-luminescent panels (see Fig. 7).

I. Access and Alignment

As can be seen from the assembly diagrams (see Figs. 2, 3, 20), access to the magnet was somewhat encumbered, the only openings being two 20" holes, one filled with the Cherenkov counter and I counters and the other with the K beam, degrader, optics, spark chambers, cables, and light pipes. Hence whenever any apparatus within the magnet needed attention, the removable downstream pole tip was backed out on a railroad track assembly, christened the "Homermobile" after its designer, Homer Allen (see Fig. 10). Moving with and attached to the pole tips were the Cherenkov counter, the barrel of I-counters, the downstream outer radius optics, and the large cylindrical chamber stereo mirror.

Removal of the pole tip was usually quite easy. Re-insertion was typically a slow process of aligning and jacking the ten-ton device such that the I-counters, with 1/4" clearance, passed into the large cylindrical chamber and around the lead cylinder, and the pole tip, with 1/16" radial clearance, passed into its hole. Shims were placed between the sides of the pole piece and the hole surface to align the optical system to within

.015" (measured radial repositioning error). The position along the beam line was always the same, as the pole tip was bolted into place, and at maximum field the force on the pole tip was nearly 600 tons.

IV. DATA ANALYSIS

A. Scanning and Measuring

170,000 photographs were scanned on SASS (Semi-Automatic Scanning System), a DDP-24 (8K core) controlled precision CRT film scanner with a 6μ minimum step size developed by the Lofgren Group. A track-selection algorithm was developed for the scanning program "MISSION IMPOSSIBLE":

1. A fiducial scan (see Fig. 7) gave a grid set-up with four data box fiducials as the masters for each frame. In reference to the data box, coordinates were measured for four fiducials mounted at a radius of 6.25" for cylindrical chamber scanning, four beam chamber fiducials and eight gap marks and eight fiducials for each outer radius pair of chambers.
2. In each frame the data box was scanned and recorded. The large cylindrical chamber was scanned as an eight-gap, sixteen-sided chamber, seeking exit and return tracks. If exactly four "tracks" were found with reflections (fainter "tracks") on the clockwise side of the heavier tracks and within an acceptable distance interval, SASS automatically proceeded to the outer radius chambers. If three or five or more "tracks" were found, SASS called the operator for "help", which was given by light pen. If two or fewer "tracks" were found, the event was rejected, recording only the data box.

3. Having had the proper "tracks" selected SASS proceeded to scan the four outer radius chambers opposite the large cylindrical chamber sparks, in which chambers outer radius tracks were likely to be found. Then the beam chamber was scanned. If on any outer radius or beam scan more than one track was recorded, "Help" was called.
4. The small cylindrical chamber was scanned and all information recorded.
5. A single 125-word record was written on tape for each event.

The minimum spark size necessary to record a spark was three successive hits, or 18μ. In the worst case of a 300:1 demagnification, this leads to a minimum track resolution (spark diameter) of 6 mm. The average was six bits, or 11 mm resolved.

B. Spatial Reconstruction

Spark tracks were reconstructed in the program KEREC in the CDC 6600 at a rate of 15 events/second. Spark widths were calculated from knowledge of the number of SASS hits and the demagnification, to obtain experimental variances.

The large cylindrical chamber and small cylindrical chamber measurements were relatively simple, with

$$Z_{LCC} = D \tan 14^{\circ} + Z_s$$

where D = separation of track and reflection and Z_s = position of stereo mirror.

The outer radius reconstruction was considerably more complicated (fish don't seem to have much trouble with fisheyes -- only people. . .).

The basic equations (see Fig. 8, 9) are

$$\rho \sin [(\beta + \alpha)/_2] = \ell \tan \alpha [1 + (\rho/\ell) (\cos [(\beta + \alpha)/2] - 1/2)]$$

and

$$\epsilon = \rho \cos [(\beta + \alpha)/_2] - \rho/2 - \rho \sin [(\beta + \alpha)/_2] \cot (\beta)$$

ρ = radius of fisheye = 2.5"; ℓ = distance to achromatic lens $\cong$ 50.4"; β = angle of ray crossing optic axis near the focal point, missing by distance ϵ; and α = angle of incidence of ray to achromatic lens. These equations can be approximated to .01% accuracy for $\alpha \leq .02$

$$\sin (\beta/2) \approx [(\ell \tan \alpha)/_\rho] [1 - .25 (\ell \tan^2 \alpha)/_\rho]$$

and

$$\epsilon = .712" \sin^2 (\beta/2) - .036"$$

Calculation of spatial position from these equations and a knowledge of the geometry of the magnet is a simple but tedious process and will not be reproduced here.[11] (See Appendix.)

Sparks which were calculated to fall outside the chamber were found to be due to double tracks in the chamber and were discarded.

For a preliminary orbit fit, a parabolic fit in r–z and a cardioid fit in r–θ were made for each event and events with too large a χ^2 in the fit (~1000 with 6–18 degrees of freedom) were checked, dropping the spark which raised the χ^2 most, and refitted, in order to lower background from extraneous sparks.

C. Momentum Reconstruction

Spatial data from KEREC and smoothed magnetic field measurements on a 1" x 1" grid were input to KEMOM which utilized the subroutine set ORBIT–ARKINT–FUNCT–FIELD to step-integrate orbits in the magnet.

Orbits were started at a point calculated to be the maximum cylindrical radius of the orbit, hence Pr = 0. Initial conditions with this constraint were a momentum estimated from the vector potential at the maximum radius, a Pz/Pθ, and spatial coordinates, calculated mainly from outer radius data.

The orbit was shot in cylindrical coordinates with a continuous momentum loss corresponding to muon momentum loss in ~ 1" steps, first "ahead" in time, then "backwards", ending at the radius of the LCC tracks. Five orbits, separately varying P_θ, P_z, r_o, θ_o, and Z_o, were shot to calculate derivatives and a χ^2 minimization procedure was followed, stopping when χ^2 changed by less than .05 χ^2. When such an orbit was reached, the orbit was continued back to the stopper within the Cherenkov counter, with continuous loss inside the gas and discrete losses in the walls and stopper. For correction for the energy loss in the stopper, an approximation to the position of the K decay was made. The orbit was run into the center of the magnet (using cartesian coordinates, as orbit trajectory solutions in cylindrical coordinates involve a (1/r) term which causes errors near r = 0 for discrete integration techniques). The beam chamber spark was extrapolated to the region of the orbit and the point on the orbit nearest the extrapolated beam track was chosen. This process had an average error of 0.25" or 1.4 MeV.

All data calculated by KEMOM, as well as input data from KEREC, was packed into 20-event (3300 word) records on tape for further processing. All data was then stored on the IBM Mass Storage System (MSS or chipstore).

All accepted data was histogrammed and various cuts applied, requiring events: a) to come from the stopper, b) to have a track in

each view of beam chamber, c) to have proper run-frame sequencing (for rescanning), and d) to have $\chi^2/N < 3.5$ (χ^2 expected = 1 per degree at freedom, with siz parameters fitted and a minimum N of eight, a minimum of two constraints per fit.) Events with N = 6 were checked and rescanned if scanning error was evident.

Processing was found most convenient in the 400 ft. film rolls in which the data was gathered and scanned, as KEMOM took ~ .3 central processor seconds per reconstructed event, or 2000 seconds per run set on the computer.

D. Rescanning

(See Tables 2, 3)

All events taken with E required in the trigger with reconstructed momentum Po > 235 MeV/c were rescanned to check the small cylindrical chamber and the general frame for μ or e signature. The particle trajectory entered the lead cylinder approximately normal to the surface of the cylinder. Muons continued through the cylinder, losing energy, scattering through small angles, and emerging at the inner side. The region of the small chamber (with respect to the large cylindrical chamber return track) into which some 95% of the muons passed was called the "mu corridor" (see Fig. 12A). Events with two tracks in the proper position in the small cylindrical chamber in relation to the large chamber sparks were called "identified muons" or "μ" (e.g., in Fig. 12A, events with abcd, abef, abgh, but not abch or abgd). Events with only one track near the return spark (e.g., abc, abe, or abg) were called "μI" for "muon in". Events with one spark opposite the return spark (e.g., abd, abf, or abh) were labelled "μO" for "muon out". Sets of small

chamber sparks which showed a track outside the "corridor" (e.g., abw or abx) were labelled "μW" for "wide-scattered muon". If either no tracks appeared to be very small radius, as would be expected from a shower-produced low energy electron, the vent was called an "e". Borderlines between the "e" designation and "μI", "μO", and "μW" were often quite hazy, such that in the end these three infrequent classifications were grouped with "e", and the background subtraction applied to the enlarged group.

This examination was done on a scanning table by the author. One-fifth of the events were rescanned a second time to check for scanning biases.

V. RESULTS

A. Backgrounds

1. Non-K Decays

All events in the KOE$\bar{M}$ and KOEM samples are apparently from K decays (see Fig. 13), with the major contribution from $K \to \mu\nu$, and also events from $K \to e\nu$, $K \to e\nu\gamma$, $K \to \pi^o e\nu$, and $K \to \pi^+\pi^o$. Two specific backgrounds were checked, by running only π mesons or protons in the beam, and by changing the π/K ratio by a factor of four. Neither effect produced any significant background.

2. Muons with Delta Rays

The KOE$\bar{M}$ and KOEM suffered a second problem causing a widening of the Kμ2 peak. The μ's emerging from the stopper can produce δ rays of a maximum energy of 5.5 MeV, while electrons are counted above 2.5 MeV. Hence μ's which lose 2.5 MeV or more in addition to normal energy loss in either the stopper or the ethane may have knocked out a δ-ray causing a pseudo-electron $K\mu_2$ peak some 2.5 MeV lower in energy than the "pure" $K\mu_2$ peak. Using a δ-ray spectrum

$$N(E) = .\frac{015}{E}\left(\frac{1}{E} - \frac{1}{E_{max}}\right) \text{ electron gm}^{-1}\text{ cm}^2\text{ MeV}^2$$

we find that .001 of the μ's leak through into the KOE and KOEM event sample, approximately the size of the hump on the low momentum $K\mu_2$ peak (see Fig. 14, 15). Such δ-rays are unfortunately captured in a magnetic bottle and carried downstream towards the Cherenkov phototubes, merrily radiating until they reached the Cherenkov limit, after an average of 20 cm.

3. $K\mu_2$ Background Subtraction

Resolution of events rescanned (see Tables 2, 3) was made into two bins, of identified μ's and of questionable μ's (μI, μO, μW) and e's. It was assumed that all background for Po > 235 was due to $K\mu_2$ secondaries. This assumption is reasonable from several standpoints. In Fig. 19 some KOE events are shown, along with the rescanned data showing contributions to the e rate from all sources. The $K\mu_2$ peak and the rising Ke_3 spectrum (cut off by the lower end of the resolution curve) are consistent with the known rates. π mesons at 245 MeV/c have a range such that they would be identified as μ's, even if π's were producing a significant number of orbits. It was further assumed that the spectrum of identified μ's was equivalent to the spectrum of μ's leaking through into the e candidate sample (i.e., the only inefficiency was the SCC track recording). Given the previous assumption, this will only have errors from statistics.

The background subtraction was made by fitting over the five 1 MeV/c bins, 235–236 to 239–240. This was done separately for $KOE\bar{M}$ and KOEM event types (see Tables 2, 3, Figs. 14, 15). While the errors in the fit may be large (3 S.D. effect = 15%), due to the rapid fall of the $K\mu_2$ peak, the effect on the branching ratio is less than 2%. Due to the unforeseen problem of δ-rays counting in the Cherenkov counter, thus changing the $K\mu_2$ spectra for KOE vs. KOG, the KOG and KOGM events could not be used as a normalization.

The χ^2 curves for a variety of different event sets are given in Fig. 11.

After the muon background subtraction, 67 ± 10.8 events remained as Ke_2 electron candidates (see Table 4, Figs. 17, 22).

4. $K \rightarrow e\nu\gamma$ Background (non-bremsstrahlung)

This experiment also measured the decay $K \rightarrow e\nu\gamma$, utilizing scintillators covered with one radiation length (.25") or lead over .26 of 4π solid angle (see Fig. 2). Decays of this type should have the γ-ray of high energy and highly collimated opposite to the electron direction.[14] The calculated efficiency for detecting the γ when the electron is captured is .45. The four events in the region $P > 240$ MeV/c with trigger KOEG indicate a contamination of 4.4 ± 2 events in the $K \rightarrow e\nu$ sample, reducing the number of events from 67.0 ± 10.8 to 62.6 ± 11.0.

B. Error Calculations

1. Momentum Width

The momentum width of 7 MeV/c FWHM is explained mostly by spark size (see Fig. 14). The average outer radius spark had a measured size of 11 mm in the radial direction, while the z size was 7 mm, due to the unfortunate property of our optical system to measure the z with the close fisheye and the r with the far one. Of course the momentum is determined mostly by r, which is approximately perpendicular to the field lines. The large cylindrical chamber, to capture two tracks in the presence of background and due to operating in a 19 kilogauss field, had to be pulsed with a longer and higher voltage pulse than those which produce fine sparks. The outer radius chambers suffered a similar but lesser problem in 15 to 17 kg. The result was, of course, bright but fat sparks,(the large cylindrical chamber average spark width was 8 mm) very good for scanning machines but poor for accurate track determination. A calculation of the momentum width broadening

due to this effect, using a uniform field and circular orbits for simplicity, yields $P/P = \pm 1.5\%$.

2. Random Cherenkov Counts

In calibration $K\mu_2$ running, 14 E triggers were recorded in coincidence with 5946 $K\mu_2$ orbits. This corresponds well with an observed leak through rate of .0025 in Ke_2 running. The total $K\mu_2$ leak–through rate is then .0035.

3. Entymological Problems

The 5946 $K\mu_2$ calibration events (see Fig. 14) is an under estimate by 5.5 ± 1%. The calibration runs were taken at the start and end of each roll of film. The data was read into the momentum reconstruction program in one–event records and read out packed in 20–event record. A programming error ended the program after the last event was input, without clearing the output buffer. This lost 12 ± 2 of 180 reconstructed $K\mu_2$ events per roll of film. 10.8 of these would have fallen within the $K\mu_2$ event distribution. Hence the number of $K\mu_2$ events for calibration is 6270.

4. Magnet Setting

The $K\mu_2$ peak in all Ke2 running is 233.7 MeV/c, 1.9 MeV/c lower than the accepted value, indicating a magnet measurement normalization error of .008. This lowers the Ke_2 effective momentum from 246.9 to 245.0 MeV/c.

5. Electron Recognition

From triggers of the type KOEG$\bar{M}$ AND KOEGM in the region below 225 MeV/c, which includes only e^+ from Ke_3, a rejection rate of 2/202 was found for scanning in the small cylindrical chamber.

Cherenkov counter efficiency was found to be 98.4 ± .2 in a beam test and is quite consistent with the 1483 Ke_3 events in the momentum region 146–162 MeV/c (see Fig. 18), expecting 1490 ± 50 from the $K\mu_2$ rate and published branching ratios.[12]

6. Resolution

The momentum spread of the muon decay secondaries measured at the Ke_2 and $K\mu_2$ settings was 7.1 MeV/c FWHM. This width was taken for the curve generated to fit the Ke_2 spectrum.

7. Bremsstrahlung[13]

Outer bremsstrahlung corrections significantly reduce the observed rate. The decay secondaries passed through an average of $.0930\ ^{+.032}_{-.025}$ (errors reflect stopper size) radiation lengths of material before the midpoint of the orbit. Using the formula

$$P(E_e > E_o - \Delta E) = \int_{E_o - \Delta E}^{E_o} \frac{e^{-y}\, y^{\alpha-1}\, dy}{\Gamma(\alpha)} \simeq \frac{(\ell n\ (E_o/(E_o - \Delta E)))^{\alpha}}{\Gamma\ (1 + \alpha)}$$

where ΔE = maximum acceptable energy loss = 5 MeV

α = (radiation lengths) x $\ell n\ 2$

and integrating over the distribution of the stopping beam, .636 ± 024 of the electrons are retained in the sample.

C. Conclusions

DKM = S1 S2 S3 $\overline{C}_\pi$ S4 $\overline{M}$1 served as a normalization for all run types. The experimental detection efficiencies E_e and E_μ are calculated in Table 5. The result is then

$$R_{exp} = \frac{N_{K \to e\nu}/(DKM_e \times E_e)}{N_{K \to \mu\nu}/(DKM_\mu \times E_\mu)} = \frac{\begin{array}{l}(\text{electron events/monitor at } Ke_2 \text{ setting})/\\(\text{efficiency for detecting } Ke_2 \text{ electrons})\end{array}}{\begin{array}{l}(\text{muon events/monitor at } K\mu_2 \text{ setting})/\\(K\mu_2 \text{ muon detection efficiency})\end{array}}$$

$$= \frac{(62.6 \pm 11.0)/(72.3 \times 10^6 \times (.498 \pm .019))}{(6270 \pm 79)/89{,}956 \times .929}$$

$$= 2.32 \pm .39 \times 10^{-5}$$

Setting $R_k = R_{exp}$ and solving for $\frac{f_p}{\frac{m_e}{m_k} f_A}$ (assuming f_p and f_A relatively real, in accord with TCP) in terms of

$$\delta = \frac{R_{exp}}{\left(\frac{m_k^2 - m_e^2}{m_k^2 - m_\mu^2}\right)^2} = 2.11 \pm .35 \times 10^{-5}$$

$$\beta = \frac{m_e}{m_\mu} = 4.85 \times 10^{-3}$$

$$\frac{\delta}{\beta^2} = \frac{R_{exp}}{R_K \text{ (pure A)}}$$

$$\frac{f_p}{\frac{m_e}{m_k} f_A} = \frac{-\left(1 - \frac{\delta}{\beta}\right) \pm \sqrt{\frac{\delta}{\beta^2} - \frac{2\delta}{\beta} + \delta}}{1 - \delta}$$

$$\frac{f_p}{\frac{m_e}{m_\pi} f_A} = -.995 \pm \sqrt{.892 \pm .148}$$

$$= -.995 \pm \begin{pmatrix} .944 \; {}^{+.076}_{-.081} \end{pmatrix}$$

$$= \begin{cases} -.051 \; {}^{+.076}_{-.081} \\ 1.939 \; {}^{+.001}_{-.076} \end{cases}$$

Here, as in π decay, $f_p \cong 0$ or there is a cancellation. Many persons[15] believe the former to be true, according to the original V–A theory[16] by Feynman and Gell-Mann. Conservatively this experiment can say at the 90% confidence level that

$$\left| \frac{f_p}{f_A} \right| < 2.10 \times 10^{-3}$$

and that assuming TCP invariance, either

$$1.90 \times 10^{-3} < \left| \frac{f_p}{f_A} \right| < 2.10 \times 10^{-3}$$

or

$$0 \leq \left| \frac{f_p}{f_A} \right| < 1.67 \times 10^{-4}$$

The corresponding limits for the pion are[17]

$$\frac{f_p}{\frac{m_e}{m_\pi} f_A} = \begin{matrix} .007 \pm .013 \\ -1.97 \pm .013 \end{matrix}$$

Direct comparison of $|f_p/f_A|$ is impaired by the arbitrary nature of the mass dividing the momentum transfer to the lepton pair, which we have taken to be the mass of the decaying meson in each case.

ACKNOWLEDGMENTS

Many people have contributed heavily to this experiment. I shall attempt only a brief list:

Design: Ken Lou, Addison Lake, Homer Allen.

Production: Bob Everett, Homer Allen, Jim Byce and the Building 25 personnel.

Beam: Tom Elioff, and a fine and extremely patient, understanding Bevatron Crew.

Programming: Joan Tyson, Leo Vardas, John Colonias.

Scanning: Peter Bergel, Steve Donelan, Sam Jones.

Throughout the experiment the Lofgren Research Group has given great support, with special thanks to David Newton, Bill Wenzel, Roy Kerth (at 3:00 A.M. especially), Al Clark, Tom Elioff, Bruce Cork, Fred Goozen, Gerry Schnurmacher, the secretaries who have run the group so efficiently, Anna Mae Naranjo Morrish and Peggy Fox, and the many others too numerous to mention.

Moral and immoral support from Chris Wright and her family, and from Jackie Berg → McReynolds, Peter Bergel, and our family, the commune and Church of Ithilien, the Berkeley Motorcycle Club Wednesday Night Nude Encounter Group, and last but not least, the LRL police staff who protected us from harm by keeping our frisbee matches off the Bevatron experiment houses and locked my door when my two pet rats got loose.

This work was done under the auspices of the U. S. Atomic Energy Commission.

FOOTNOTES AND REFERENCES

1. D. R. Bowen, A. K. Mann, W. K. McFarlane, A. D. Franklin, E. B. Hughes, R. L. Imlay, G. K. O'Neill, and D. H. Reading, Phys. Rev. 154, 1314 (1967).

2. D. R. Botterill, R. M. Brown, I. F. Corbett, G. Culligan, J. McL Emmerson, R. C. Field, J. Garvey, P. B. Jones, N. Middlemas, D. Newton, T. W. Quirk, G. L. Salmon, P. Steinberg, and W.S.C. Williams, Phys. Rev. 171, 1402 (1968).

3. S. Gasiorowicz, Elementary Particle Physics, Wiley, New York (1966), pp 504-507.

4. N. Cabibbo, Phys. Rev. Letters 10, 531 (1963).

5. S. Berman, Phys. Rev. Letters 1, 468 (1958).

6. Toichiro Kinoshita, Phys. Rev. Letters 2, 477 (1959).

7. Ya. A. Smorodinskii and Hu Shih-K'e, Soviet Physics J.E.T.P. 14, 438 (1962).

8. To be published, Nuclear Instruments and Methods, J. F. McReynolds, D. Newton, W. A. Wenzel.

9. J. Colonias, LRL-Berkeley (private communication).

10. L. Vardas, R. Belshe, LRL-Berkeley (private communication).

11. W. A. Wenzel, LRL-Berkeley, Bevatron Report No. 953 (1967).

12. D. R. Boterill, R. M. Brown, A. B. Clegg, I. F. Corbett, G. Culligan, J. McL. Emmerson, R. C. Field, J. Garvey, P. B. Jones, N. Middlemas, D. Newton, T. W. Quirk, G. L. Salmon, P. Steinberg, W.S.C. Williams, Phys. Rev. 174, 1663 (1968).

13. W. Heitler, The Quantum Theory of Radiation, Clarendon Press, Oxford (1954), pp 368-382.

14. B. Barrett, RHEL (private communication).

– – continued

15. S. Berman, SLAC; "Feynman is always right." (private communication).

16. R. P. Feynman, M. Gell-Mann, Phys. Rev. 109, 193 (1958).

17. E. di Capua, R. Garland, L. Pondrom, and A. Strelzoff, Phys. Rev. 133B, p. 1333 (1964).

Appendix

FISHEYE OPTICS

There are two fisheye mirrors, 1 and 2, with focal points on the optic axis $\vec{f}_i = (X_{if}, Y_{if}, Z_{if})$. (See Figs. 8, 9).

Off the optic axis, the effective focal point is

$$\vec{P}_i = \vec{f}_i + \vec{\epsilon}_i$$

$$= (X_{if}, Y_{if} + \epsilon \sin\gamma, Z_{if} - \epsilon \cos\gamma)$$

$$\gamma = \sphericalangle\,(\text{Z axis, optic axis})$$

For $\gamma = \pi/2$, $\varphi = 0$ (see Fig. A1),

[$\varphi = \sphericalangle$ (plane of spark and optic axis, plane of Z axis and optic axis)].

A line to a spark through P_i is

$$\hat{\ell}_i = (0, \cos\beta_i, \sin\beta_i)$$

For $\varphi \neq 0$

$$\hat{\ell}_i = (\sin\beta_i \sin\varphi_i, \text{vs}\,\beta_i, \sin\beta_i \cos\varphi_i)$$

For $\varphi \neq 0$, $\gamma \neq 0$

$$\hat{\ell}_i = \Gamma\, \hat{\ell}_i$$

where

$$\Gamma = \begin{pmatrix} 1 & 0 & 0 \\ 0 & \cos\gamma & -\sin\gamma \\ 0 & \sin\gamma & \cos\gamma \end{pmatrix}$$

$$\hat{a}_i = \hat{\ell}'_i = \begin{pmatrix} \sin\beta \sin\varphi \\ \cos\beta \cos\gamma + \sin\gamma \sin\beta \cos\varphi \\ -\cos\beta \sin\gamma + \sin\beta \cos\varphi \cos\gamma \end{pmatrix} = \begin{pmatrix} a_{ix} \\ a_{iy} \\ a_{iz} \end{pmatrix}$$

For a distance from $\vec{P}_i$ along line (i) of λ_i, there is a point $\vec{q}$:

$$\vec{q}_i = \vec{P}_i + \lambda_i \hat{a}_i$$

The separation s of $\vec{q}_i$ and $\vec{q}_2$ is

$$S(\lambda_1, \lambda_2) = |\vec{q}_1 - \vec{q}_2|$$

$$= \left[\sum_j (P_{1j} - P_{2j} + \lambda_1 a_{1j} - \lambda_2 a_{2j})^2\right]^{1/2}$$

$$\frac{\partial S}{\partial \lambda_i} = \frac{\sum_j a_{1j} (P_{1j} - P_{2j} + \lambda_1 a_{1j} - \lambda_2 a_{2j})}{S(\lambda_1, \lambda_2)}$$

$$\frac{\partial S}{\partial \lambda_2} = \frac{\sum_j a_{2j} (P_{2j} - P_{1j} + \lambda_2 a_{2j} - \lambda_1 a_{1j})}{S(\lambda_1, \lambda_2)}$$

Setting these equal to zero to find the relative minimum,

$$\lambda_1 \sum_j a_{1j}^2 - \lambda_2 \sum a_{1j} a_{2j} + \sum_j a_{1j} (P_{1j} - P_{2j}) = 0$$

and a similar equation with $2 \leftrightarrow 1$.

Solving these equations we find

$$\lambda_1 = \frac{\sum_j [a_{1j} - a_{2j} (\sum_k a_{1k} a_{2k})] (P_{1j} - P_{2j})}{1 - (\sum_k a_{1k} a_{2k})^2}$$

and similarly with $2 \leftrightarrow 1$.

The track position $\vec{t}$ is then

$$\vec{t} = \frac{1}{2} (\vec{P}_1 + \vec{P}_2 + \lambda_1 \vec{a}_1 + \lambda_2 \vec{a}_2)$$

with an error

$$E = \frac{1}{2} S (\lambda_1, \lambda_2)$$

to be combined with spark width to calculate the variances.

Table 1A. TYPICAL FIIM FORMAT

Run #	Type	Trigger	Purpose
1	$K\mu_2$	KO, KOG	$K\mu_2$ Calibration
2, 3	Ke_2	KOE, KOG	Data
4	Ke_3	KOE, KOG	Cherenkov Calibration
5, 6	Ke_2	KOE, KOG	Data
7	$K\pi_2$	KO, KOG	Gamma Counter Calibration
8	$K\mu_2$	KO, KOG	$K\mu_2$ Calibration

Table 1B. RUN SETTINGS AND LENGTHS

Type	Time (min)	Lengths DKM	Lengths MON	Frames	Field (kg) (M5 Center)	Coil Currents Outer (Z>8 in)	(Amp-Turns) Inner (Z<8in)
Ke_2	120	4.5×10^5	10^7	500	18.60	8.05×10^5	5.90×10^5
$K\mu_2$	4	1.3×10^3	10^4	130	18.16	7.45×10^5	5.96×10^5
$K\pi_2$	8	7×10^3	10^5	130	15.67	5.05×10^5	5.68×10^5
Ke_3	25	10^5	2×10^6	250	12.27	3.43×10^5	4.47×10^5

Table 2. KOE$\bar{M}$ EVENTS

	(1)	(2)	(3)	(4)	(5)	(6)	(7)	(8)	(9)	
p	e	e–μW	μW	μI	μ0	Tot	μ	μ*n	(6)–(8)	Error
235	9	3	31	15	6	64	138	58.5	5.5	9.1
236	18	4	26	4	4	56	136	57.5	–1.5	9.0
237	8	6	19	4	4	41	86	36.4	4.6	7.2
238	7	1	4	2	0	14	47	19.9	–5.9	4.5
239	4	0	3	1	1	9	28	11.8	–2.8	3.6
240	5	0	3	2	0	11	17	7.2	4.8	3.7
241	5	1	2	0	1	9	5	2.1	6.9	3.1
242	4	1	0	0	0	5	3	1.3	3.7	2.3
243	5	0	0	0	0	5	2	.8	4.2	2.3
244	4	0	0	1	0	5	2	.8	4.2	2.3
245	4	0	1		0	5	0	0	5	2.2
246	1	0			2	3	0	0	3	1.7
247	3	0				3	0	0	3	1.7
248	0	1				1	0	0	1	1
249	1					1	1	.4	.6	1.1
250							1	.4	–.4	1

n = normalizing constant = .423

$$\text{Error } (p) = \sqrt{\text{Tot}(p)+n^2\mu(p)}$$

Table 3. KOEM EVENTS

	(1)	(2)	(3)	(4)	(5)	(6)	(7)	(8)	(9)	
p	e	e–μW	μW	μI	μ0	Tot	μ	μ^*n	(6)–(8)	Error
235	35	5	16	94	30	180	1234	183.1	–3.1	14.4
236	19	2	18	65	27	131	866	128.2	2.8	12.3
237	19	2	13	41	9	84	571	84.7	–.7	9.8
238	10	4	4	30	2	50	349	51.8	–1.8	7.6
239	7	1	6	14	0	28	168	24.9	3.1	5.7
240	2	0	2	6	3	13	105	15.5	–2.5	4.2
241	5	1	2	5	3	16	54	8.0	8.0	4.1
242	5	1	3	4	0	13	20	3.0	10.0	3.9
243	1		0	2	0	3	10	1.4	1.6	1.9
244	3		1	1	0	5	5	.7	4.3	2.4
245	1			2	1	4	6	.9	3.1	2.1
246	0			2		2	2	.3	1.7	1.5
247	1					1	0	0	1	1.1
248	2					2	1	.1	1.9	1.5
249	1					1	1	.1	.9	1.1
250	0					0	0	0	0	1
251	1					1	0	0	1	1
252							0	0	0	1
253							1	.1	–.1	1
254							1	.1	–.1	1

n = .148

Table 4. KE_2 SPECTRUM

p	(1) KOE$\bar{M}$	(2) KOEM	(3) Tot	(4) Error	(5) Th.	(6) $\frac{(5)-(3)}{(4)}$	(7) $(6)^2$
240	4.8	–2.5	2.3	5.2	5.0	–.52	.27
241	6.9	8.0	14.9	4.7	6.7	1.74	3.04
242	3.7	10.0	13.7	4.7	8.2	1.17	1.36
243	4.2	1.6	5.8	3.0	9.3	–1.17	1.36
244	4.2	4.3	8.5	3.3	9.5	.30	.09
245	5	3.1	8.1	3.0	8.5	.13	.02
246	3	1.7	4.7	2.3	6.8	.96	.92
247	3	1	4.	2.0	4.9	.45	.20
248	1	1.9	2.9	1.8	3.1	.11	.01
249	.6	.9	1.5	1.5	1.7	.13	.02
250	–.4	0	–.4	1	.9	1.3	1.69
251		1	1	1	.6	.4	.16
			67.0 ± 10.8				9.16 = χ^2, 12 D.F.

Table 5

Detection Efficiencies for Electrons in Ke_2 Running and Muons in $K\mu_2$ Running

	Correction to E_e	Correction to E_μ
Momentum Window		
$P\mu = (228\text{–}239)$, $P\mu_o = 234.3$	.949	.941
$Pe = (240\text{–}251)$, $Pe_o = 245.0$		
U_γ		
Rare Mass	.963	1.0
Inner Bremsstrahlung and Virtual Photons	.881	.987
Cherenkov Counter	.98	1.0
Outer Bremsstrahlung	.636 ± .024	1.0
Rescanning Misidentification	.99	1.0
Product	.498	.929

Table 6. COINCIDENCE NOMENCLATURE

Name	Inputs	Function
MON	M1, M2, M3	External Proton Beam Monitor
BEV	Bevatron Pulse #33	Count Number of Bevatron Pulses
B_π	$S1_\pi$ S2	Pi Mesons in Beam
BK	$S1_K$ S2 $S3_K$ $\overline{C}_\pi$	K Mesons in Beam
DK	BK S4 $\overline{S4}_{large}$	Stopping K Mesons
DKM	DK $\overline{Mi}$	Stopping K Mesons With No Extra Beam Particles (overall normalization)
O	I_i O_j I_K	18 Triple–coincidence Systems Counting Orbits in Spectrometer Magnet Aperture and in Momentum Bite
KO	DKM, O	Orbitting Decay Secondaries from K Mesons
E	Ci, $\overline{Ci}_{large}$	Electron Signature
G	G_i	Gamma Ray Signature
KOE	KO, E	K → Orbitting Electron
KOG	KO, G	K → Orbitting Particle + γ Ray
M	M	Cylindrical Scintillator (Muon Counter)

FIGURE CAPTIONS

Fig. 1 Bevatron External Proton Beam, Channel 1, Beam 5B.

Fig. 2 M5 Spectrometer Magnet Interior – Side View.

Fig. 3 M5 Spectrometer Magnet Interior – Axial View (with typical orbit).

Fig. 4 Magnetic Field in Median Plane (as a function of radius for the four run types).

Fig. 5 Outer Radius Light Pipe Assembly.

Fig. 6 Fast Electronics Diagram.

Fig. 7 (a) Fiducial Exposure.
(b) Visible Event Exposure.

Fig. 8 Outer Radius Optics (simplified).

Fig. 9 Outer Radius Optics (in magnet).

Fig. 10 Homermobile.

Fig. 11 Chi-squared Plots
(a) Electron Candidates, $\bar{K}e_2$ Setting, $P \geq 240$ MeV/c.
(b) Muons, Ke_2 Setting, $P \geq 240$ MeV/c.
(c) Muons, Ke_2 Setting, $240 > P \geq 229$ MeV/c.
(d) Muons, $K\mu_2$ Setting, $240 > P \geq 229$ MeV/c.
(e) Electrons, Ke_3 Setting, $162 \geq P \geq 145$ MeV/c

Fig. 12 Particle Recognition in the Small Cylindrical Chamber
(a) The "Muon Corridor".
(b), (c), (d) Muons in "Muon Corridor".
(e) Typical Wide-scattered Muon (μW).
(f) Typical One-Track-In Muon (μI).
(g) Typical One-Track-Out Muon (μO).
(h), (j), (k) Typical Electron (e).

Fig. 13 Kaon Decay Lifetimes (slope of line = 12.35 ns.)
(a) All Events, Ke_2 setting.
(b) Electron Candidates, Ke_2 Setting, $P \geq 240$ MeV/c.
(c) Muons, $K\mu_2$ Setting, $240 > P \geq 229$ MeV/c.

Fig. 14 Data Samples
(a) KOE Trigger Without M Light (KOE), Ke_2 Setting.
(b) KOE Trigger With M Light (KOEM), Ke_2 Setting.
(c) DKO Trigger, All Events, $K\mu_2$ Setting.

Fig. 15 KOE Events, $P \geq 235$ MeV/c
(a) Muons (identified in SCC)
(b) Electron Candidates.
(c) Electron Spectrum (with muon background subtracted).

Fig. 16 KOEM Events, $P \geq 235$ MeV/c
(a) Muons.
(b) Electron Candidates.
(c) Electron Spectrum (background subtracted).

Fig. 17 Ke_2 Spectrum (sum of 15c and 16c).

Fig. 18 Ke_3 Spectrum at Ke_3 Setting.

Fig. 19 KOE Trigger, Ke_2 Setting (all events not recognized by computer as muons, with electron candidate spectrum).

Fig. 20 Spectrometer Apparatus (magnet open).

Fig. 21 Momentum Acceptance (at Ke_2 setting).

Fig. 22 Calculated Ke_2 Spectrum with Bremsstrahlung and Momentum window.

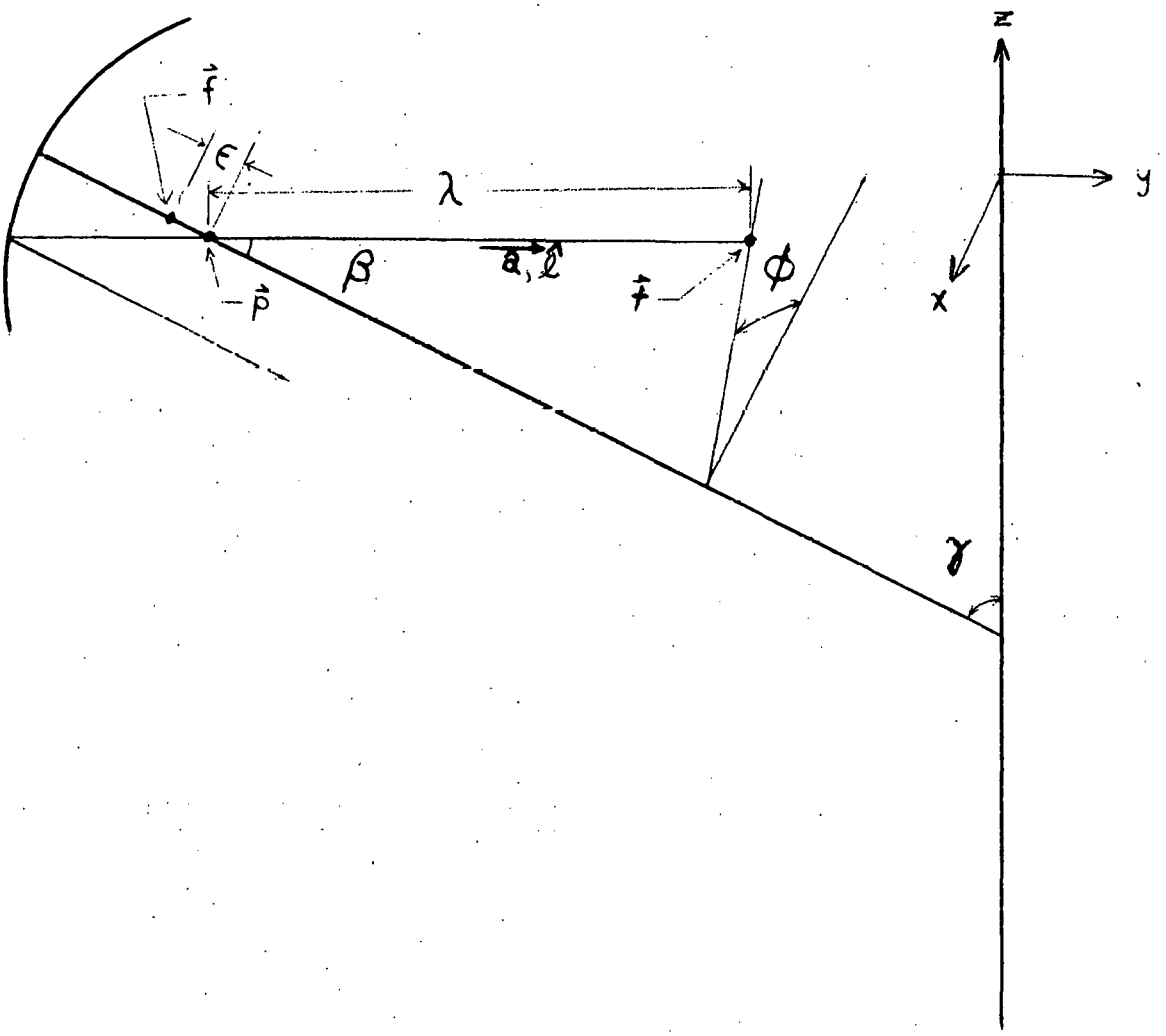
z
y
x
$\vec{f}$
ϵ
λ
β
$\vec{a}, \vec{\ell}$
$\vec{f}$
ϕ
$-\vec{p}$
γ

FIG. A1

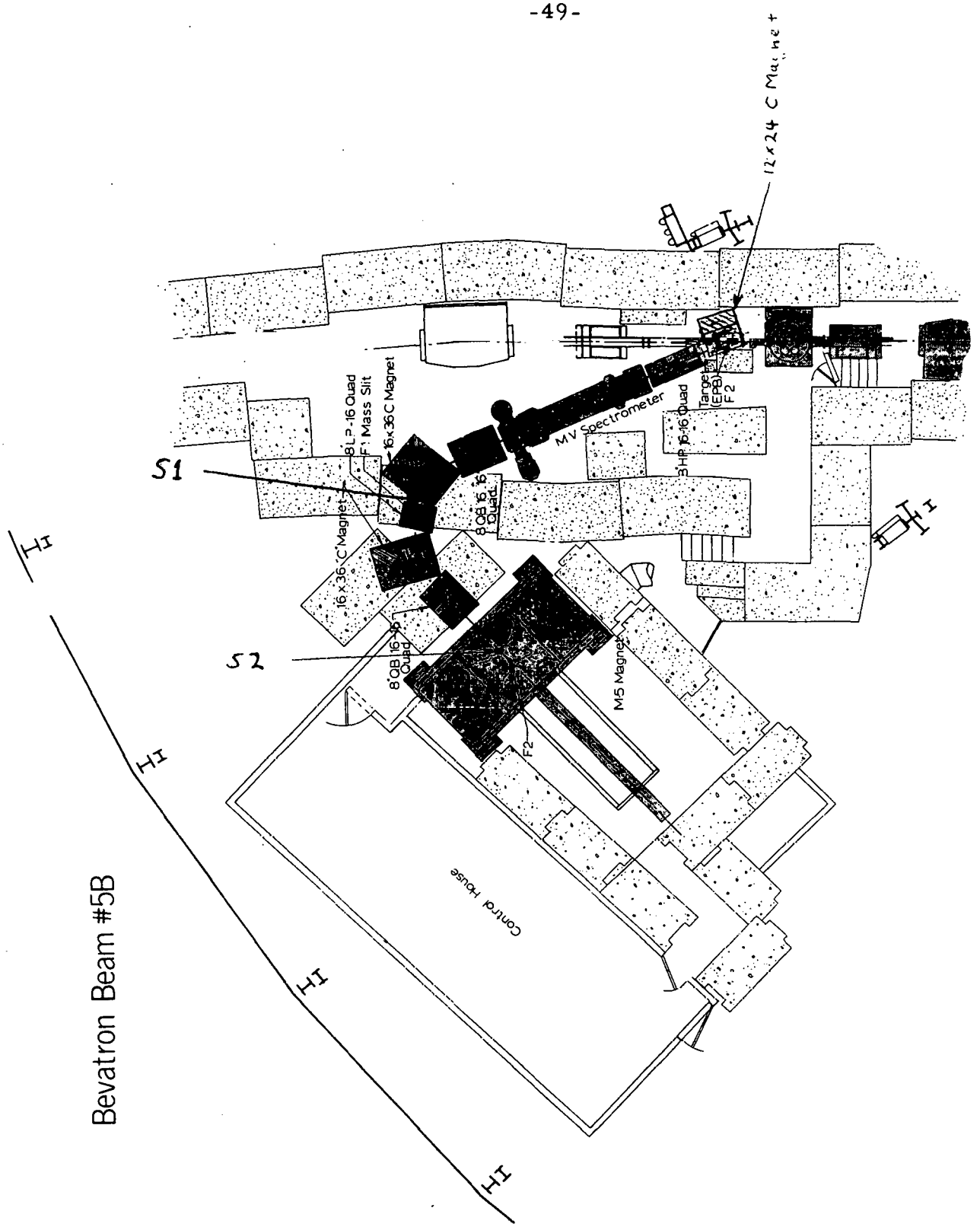
12x24 C Magnet
MV Spectrometer
Target (EPB) F2
3HP 16-16 Quad
8LP-16 Quad
F1 Mass Slit
16x36C Magnet
8QB 16-16 Quad
16x36 C Magnet
S1
S2
8QB 16-16 Quad
M5 Magnet
F2
Control House
Bevatron Beam #5B
H
H
H
H

FIG. 1

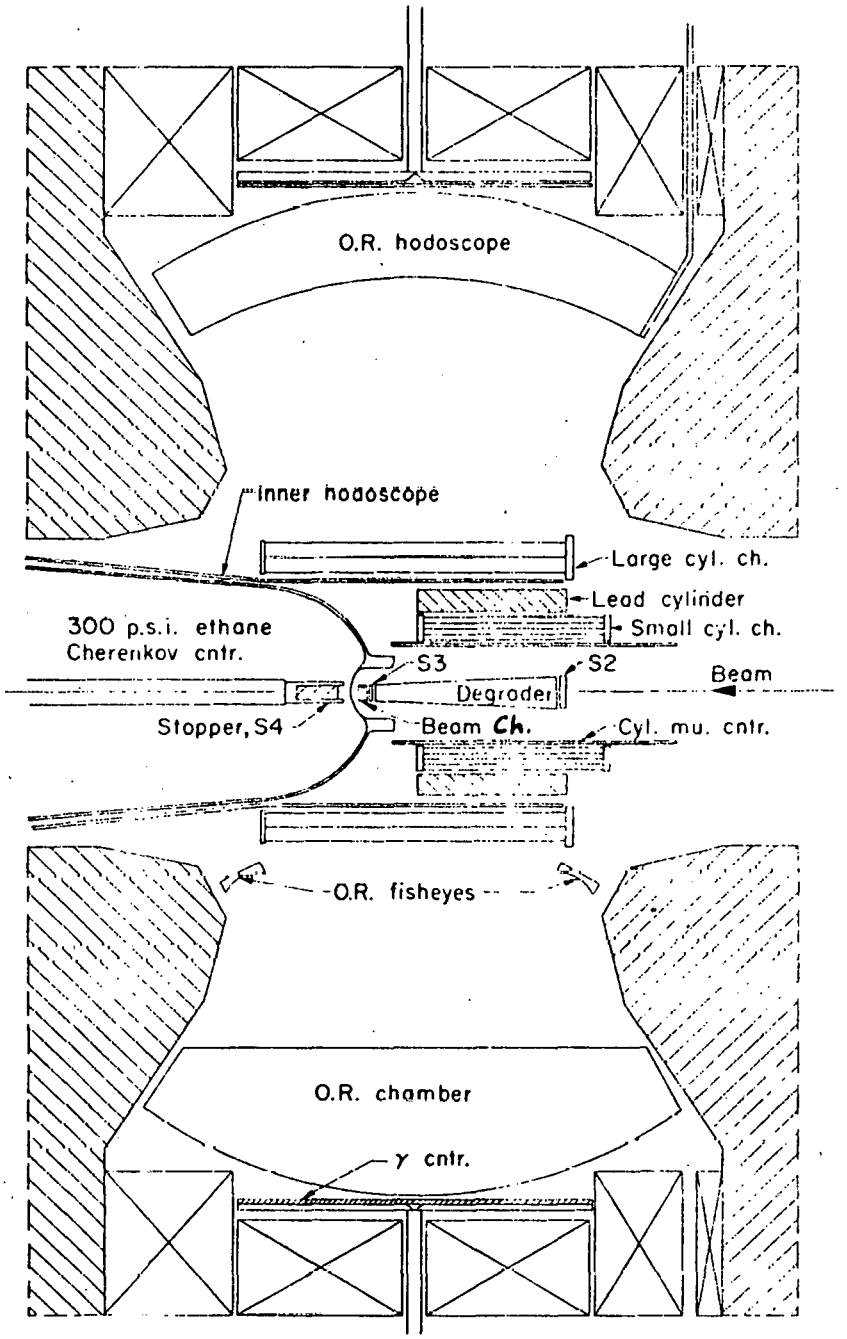

Ke2 magnet interior
(O.R.=outer radius)

XBL708-3552

FIG. 2

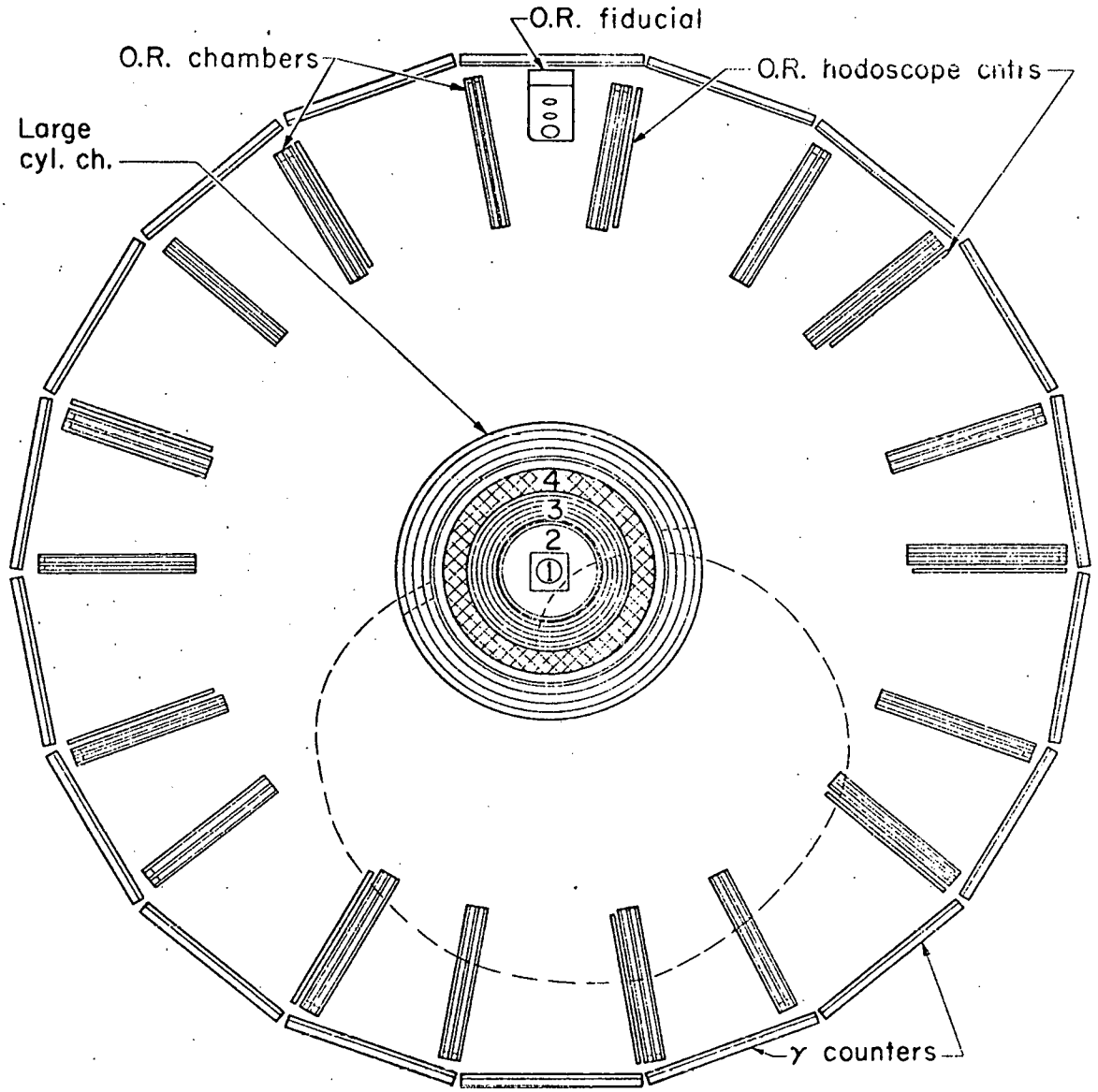

Ke2 magnet interior with typical orbit

1 Degrader
2 Cylindrical μ counter
3 Small cylindrical chamber
4 Lead cylinder

XBL708-3553

FIG. 3

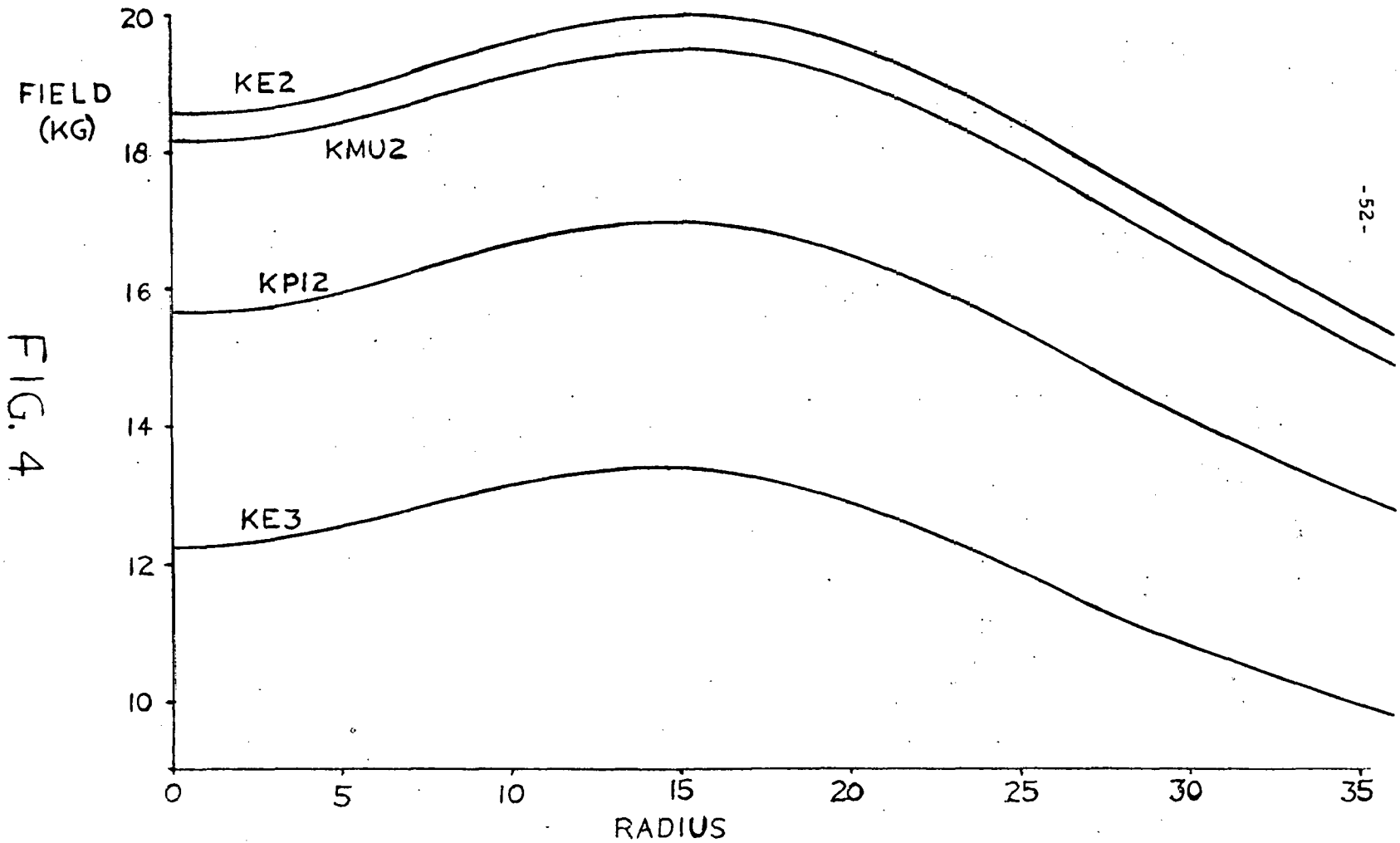
FIELD
(KG)
20
18
16
14
12
10
KE2
KMU2
KPI2
KE3
0
5
10
15
20
25
30
35
RADIUS

FIG. 4

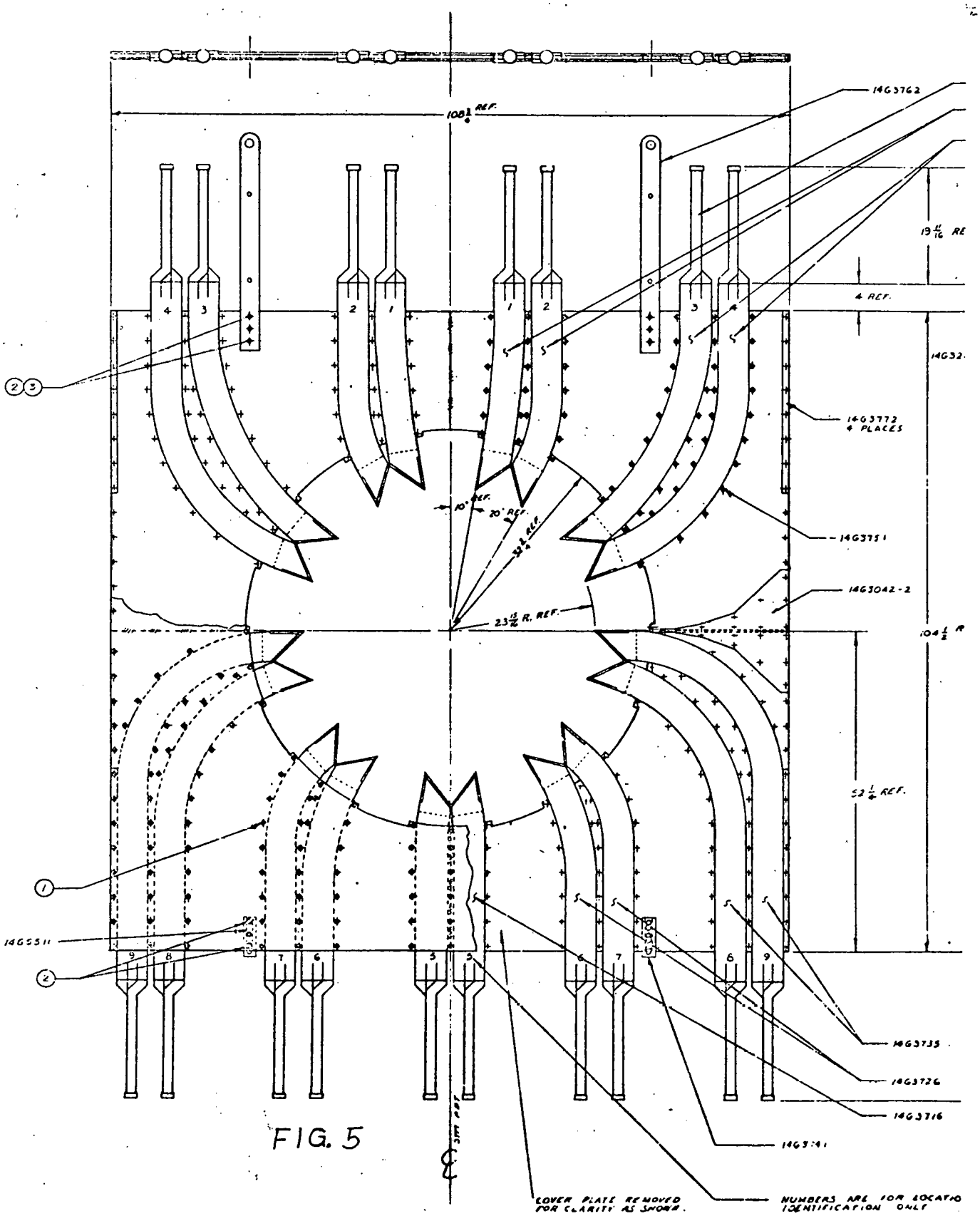
14G3762
108½ REF.
19 11/16 RE
4 REF.
14G32
14G3772
4 PLACES
10° REF.
20° REF.
14G3751
14G3042-2
23 11/16 R. REF.
104½ R
52½ REF.
14G3511
14G3735
14G3726
14G3716
14G3741
COVER PLATE REMOVED FOR CLARITY AS SHOWN.
NUMBERS ARE FOR LOCATIO IDENTIFICATION ONLY

FIG. 5

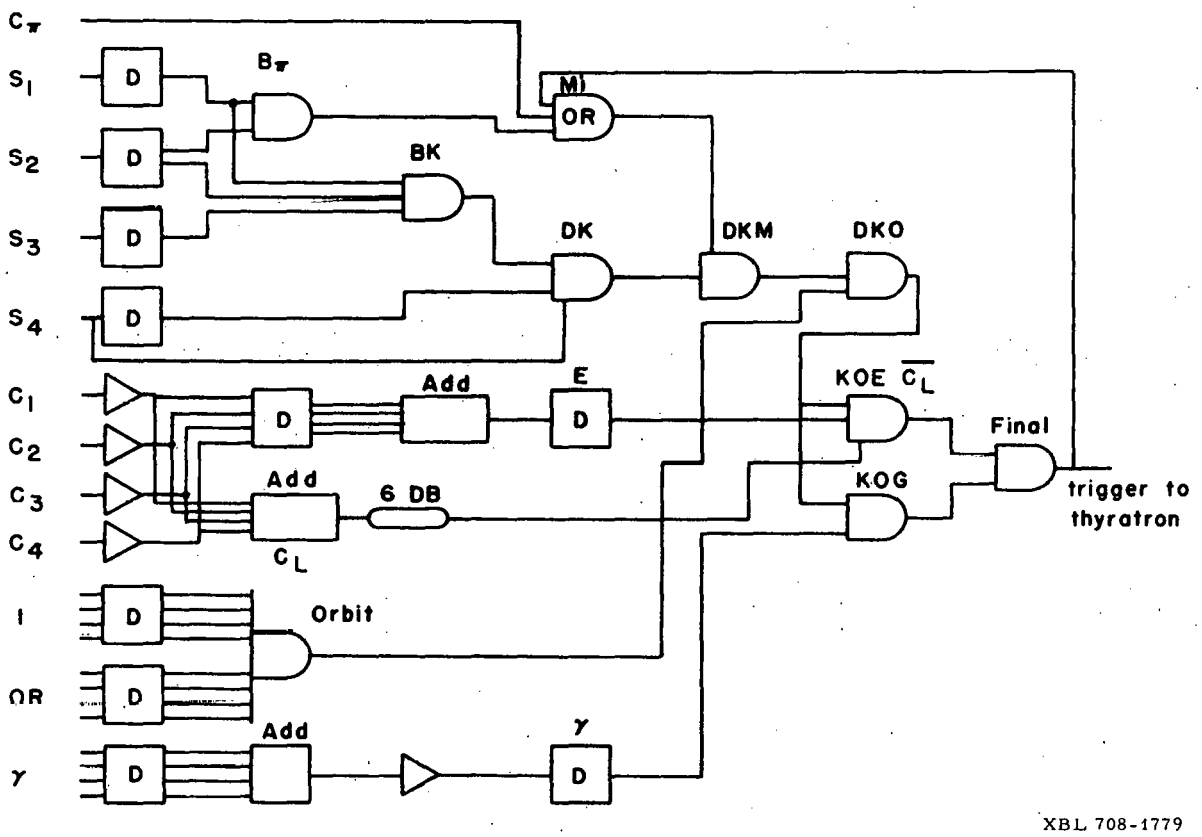
C_T
S_1
S_2
S_3
S_4
C_1
C_2
C_3
C_4
I
OR
γ
D
B_T
MI
OR
BK
DK
DKM
DKO
Add
E
KOE $\overline{C_L}$
Final
KOG
trigger to thyratron
6 DB
C_L
Orbit
γ
XBL 708-1779

FIG. 6

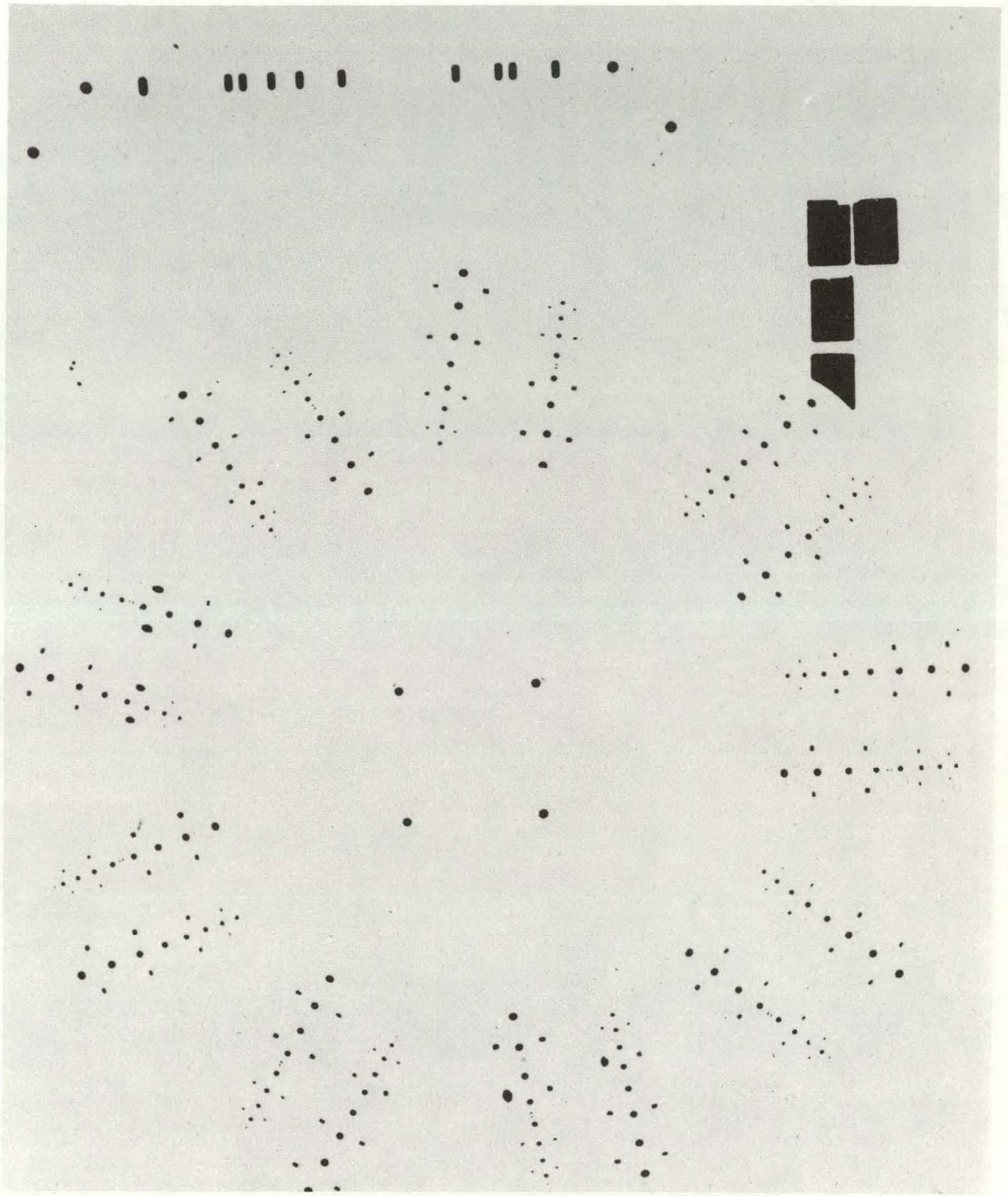

Fig. 7A

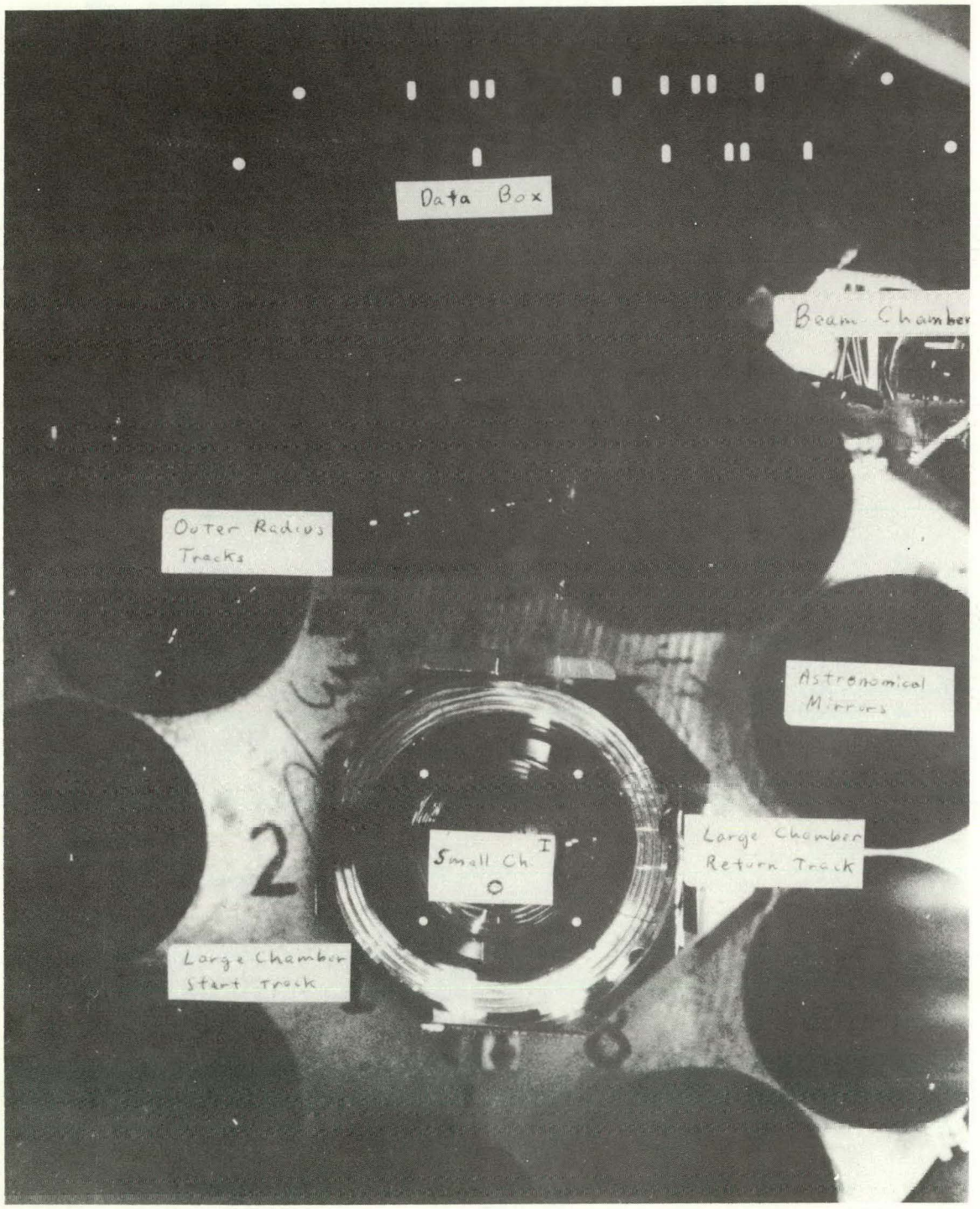

XBB 7010-4519

Fig. 7B

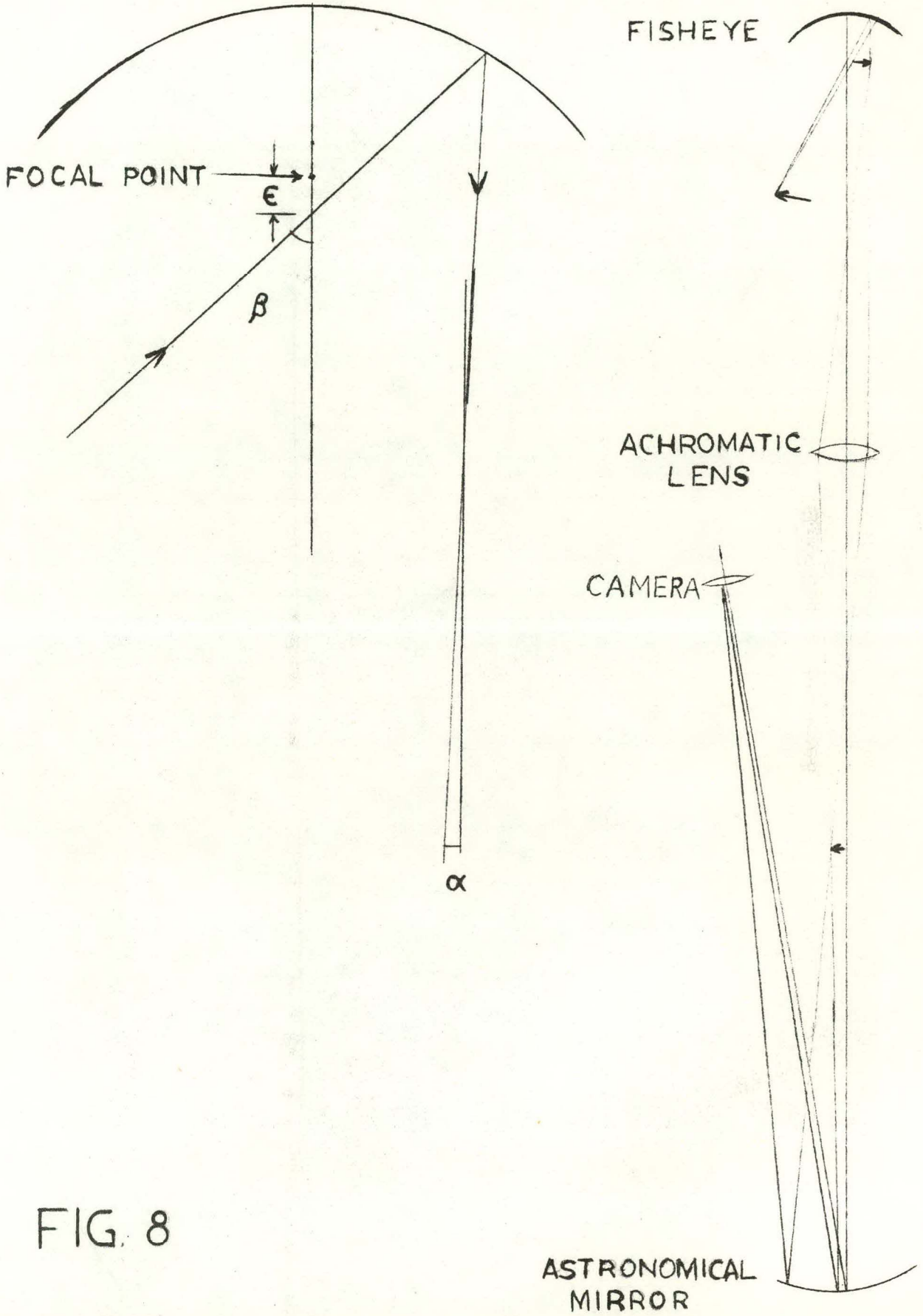
FISHEYE
FOCAL POINT
ε
β
ACHROMATIC
LENS
CAMERA
α
ASTRONOMICAL
MIRROR

FIG. 8

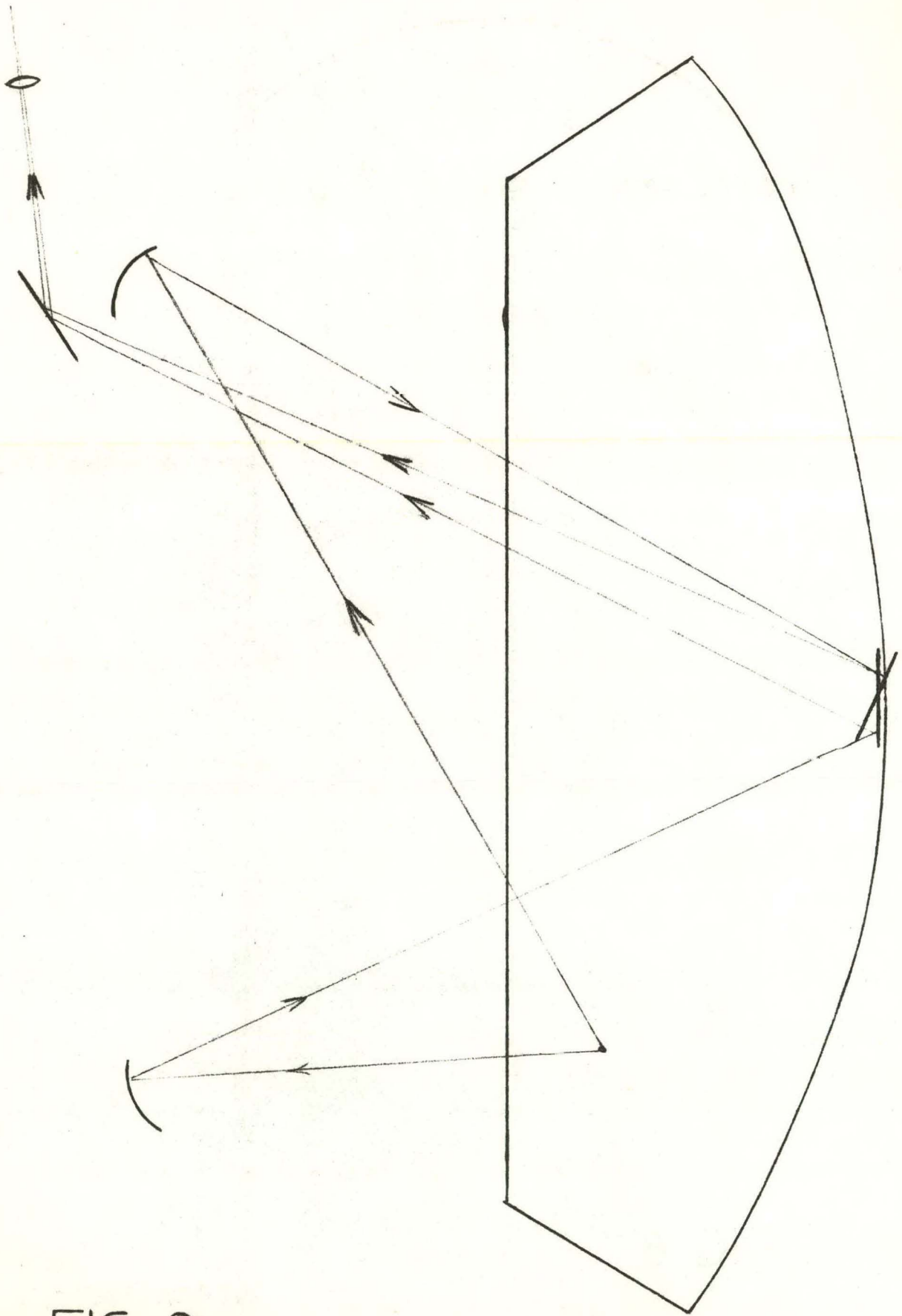

FIG. 9

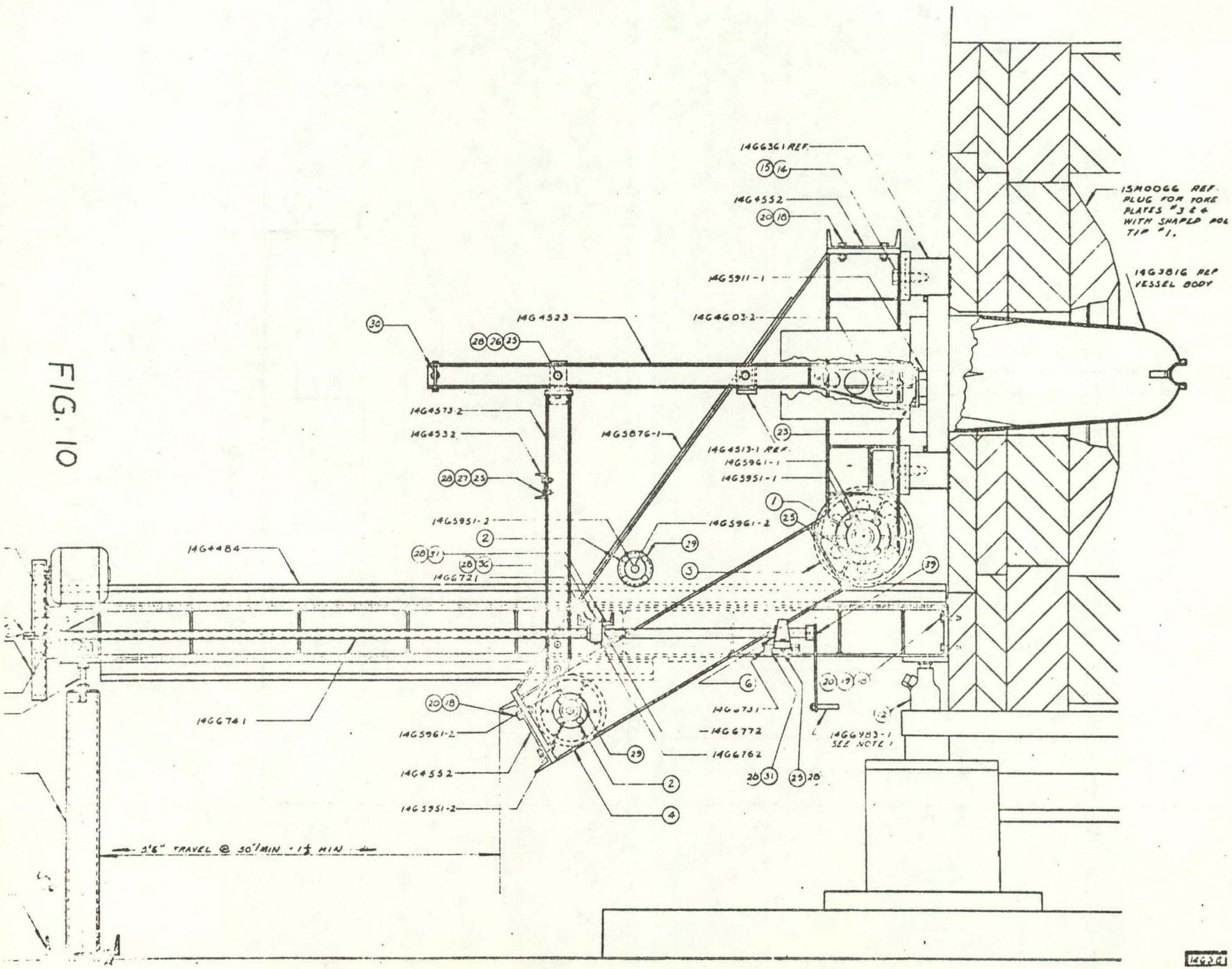
14GG361 REF.
15 16
14G4552
20 18
14G5911-1
14G4523
14G4603-2
30
28 26 23
14G4573-2
14G4532
28 27 23
14G5876-1
14G4513-1 REF.
14G5961-1
14G5951-1
1
25
14G5951-2
14G5961-2
2
29
20 31
28 30
14GG721
3
39
14G4484
6
20 19
14GG731
14GG772
14GG983-1
SEE NOTE 1
14GG762
28 31
29 28
20 18
14G5961-2
14G4552
14G5951-2
29
2
4
14GG741
3'6" TRAVEL @ 30"/MIN - 1" MIN
15M0066 REF.
PLUG FOR YOKE
PLATES #3 & 4
WITH SHAPED POLE
TIP #1.
14G3816 REF
VESSEL BODY

FIG. 10

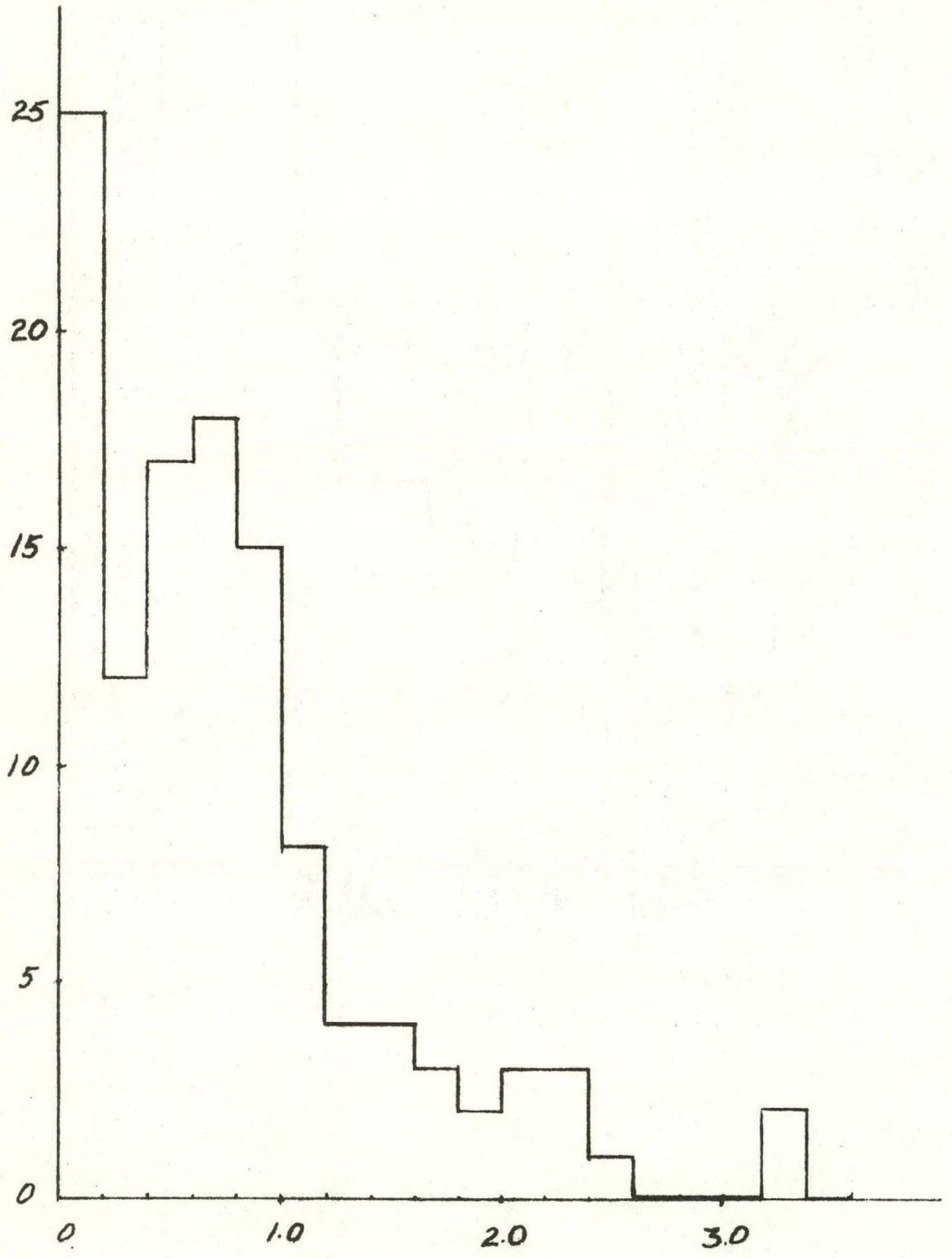

FIG 11A

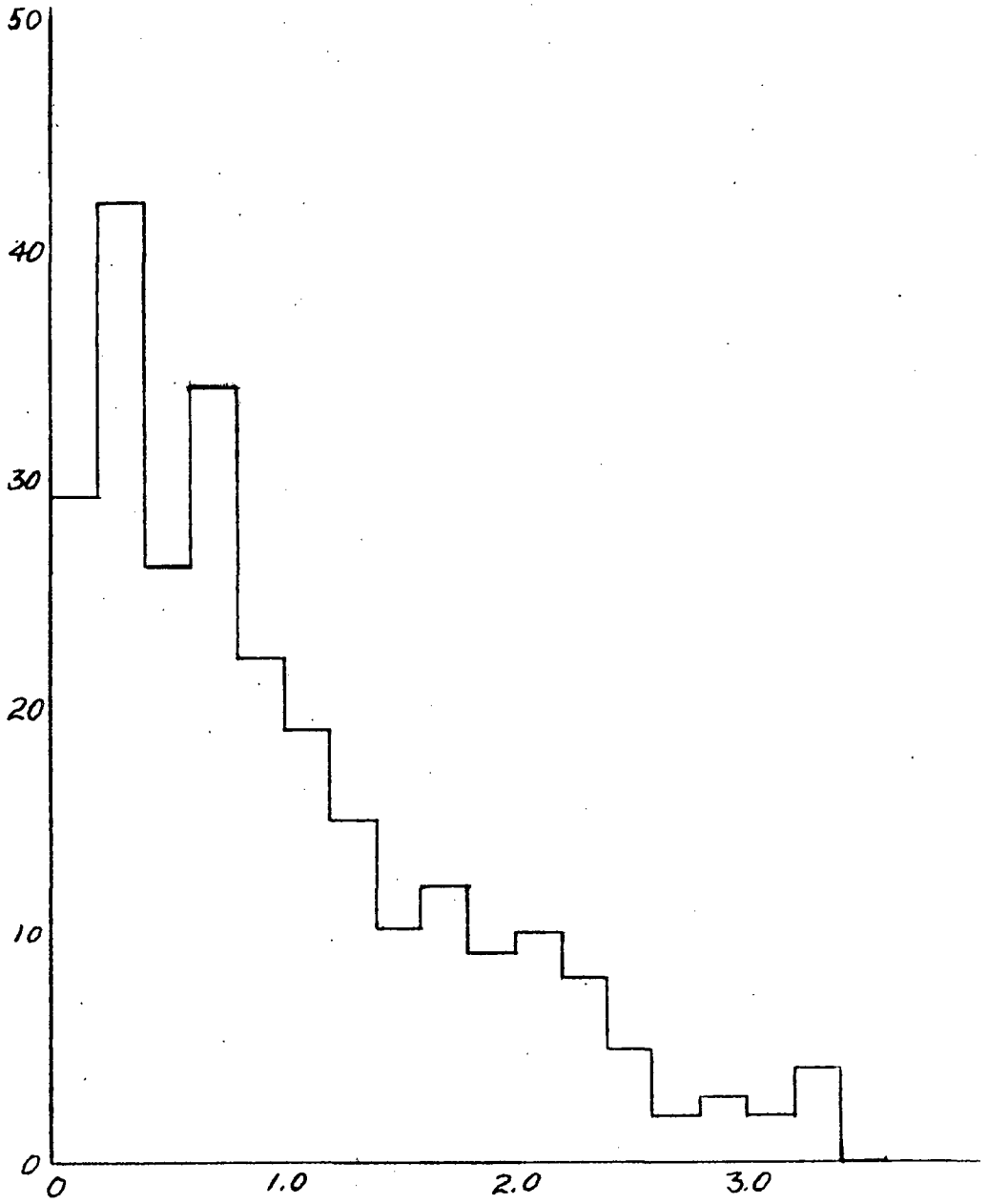

FIG 11B

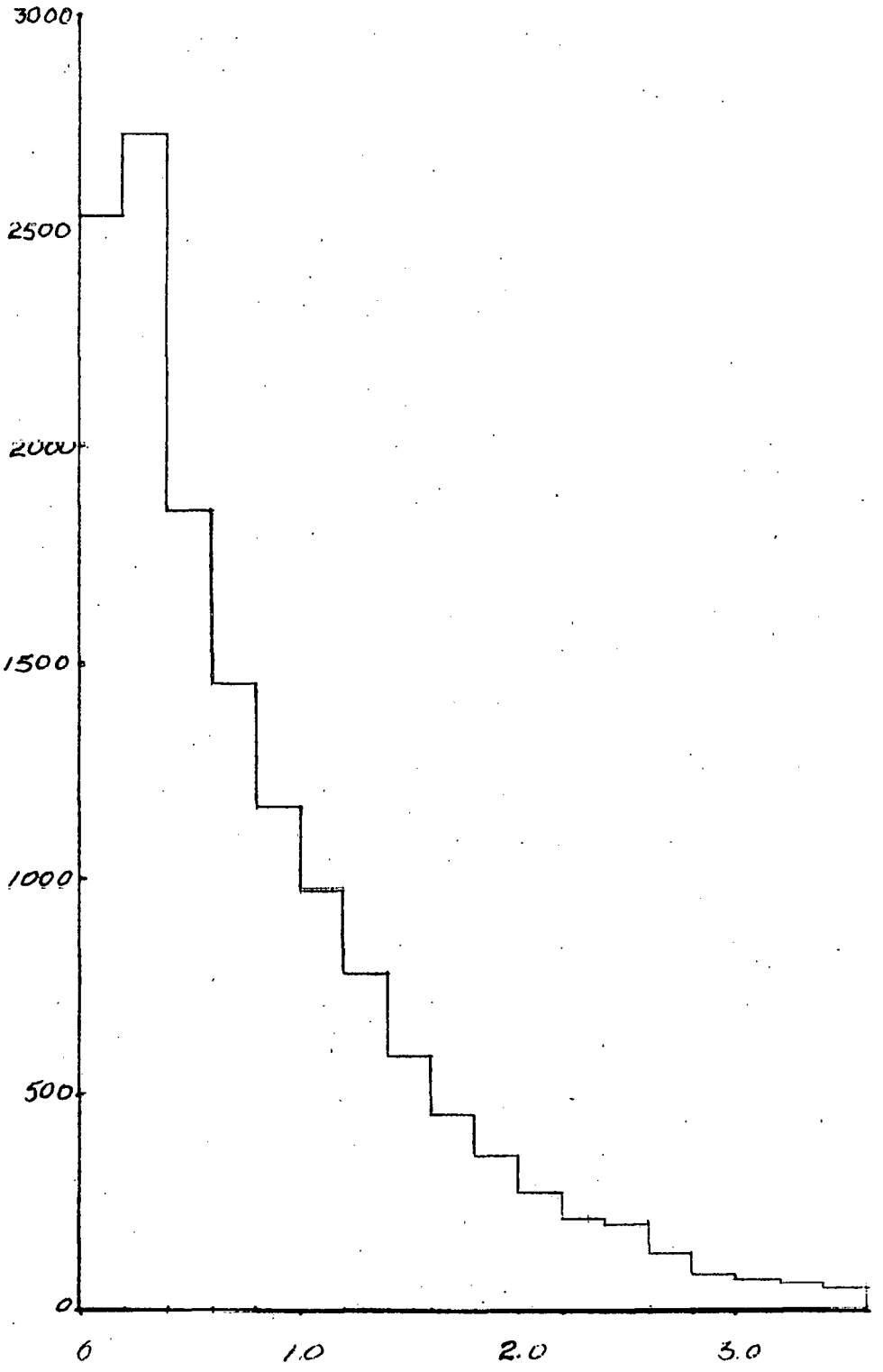

FIG 11C

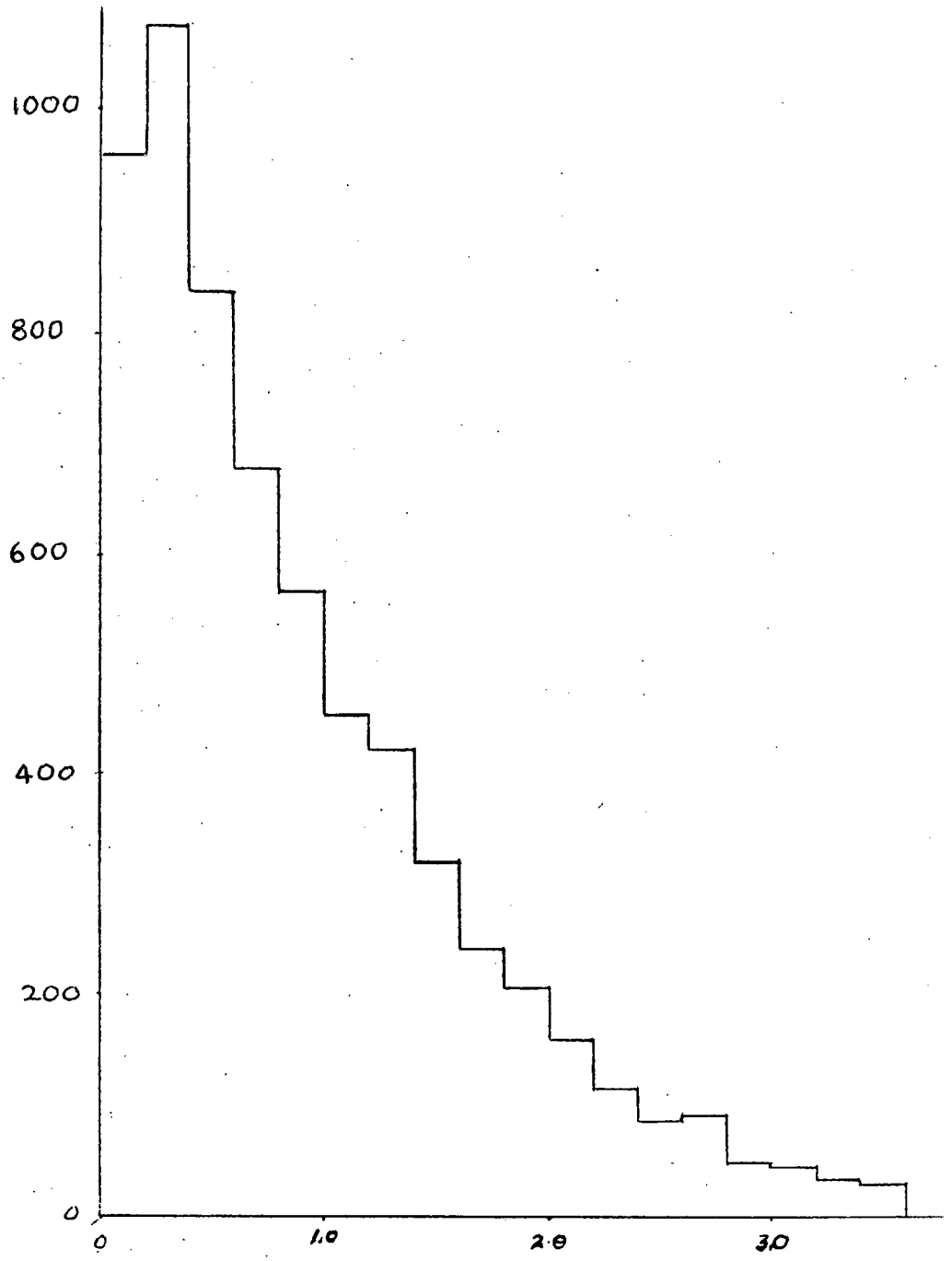

FIG. 11D

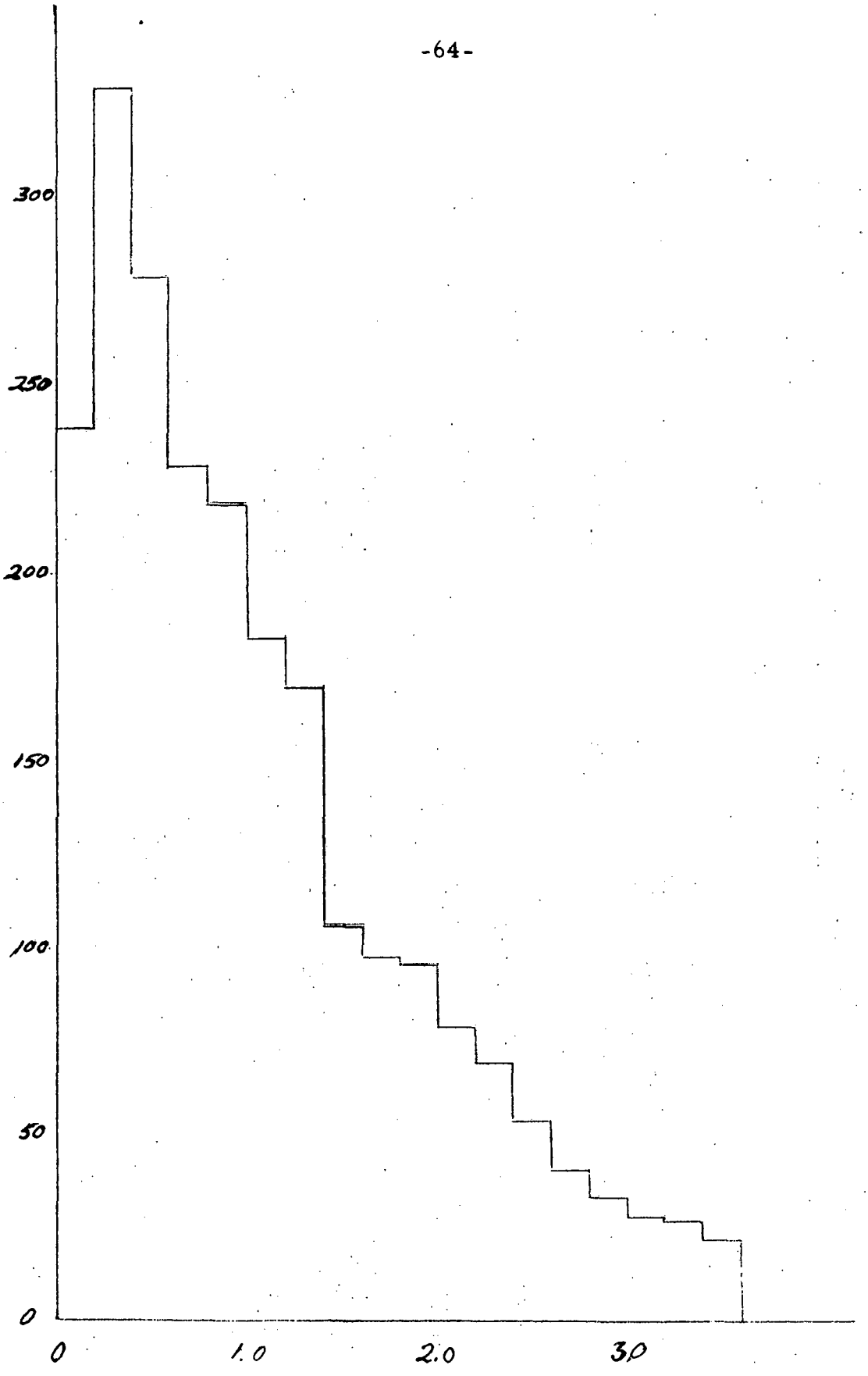

FIG 11E

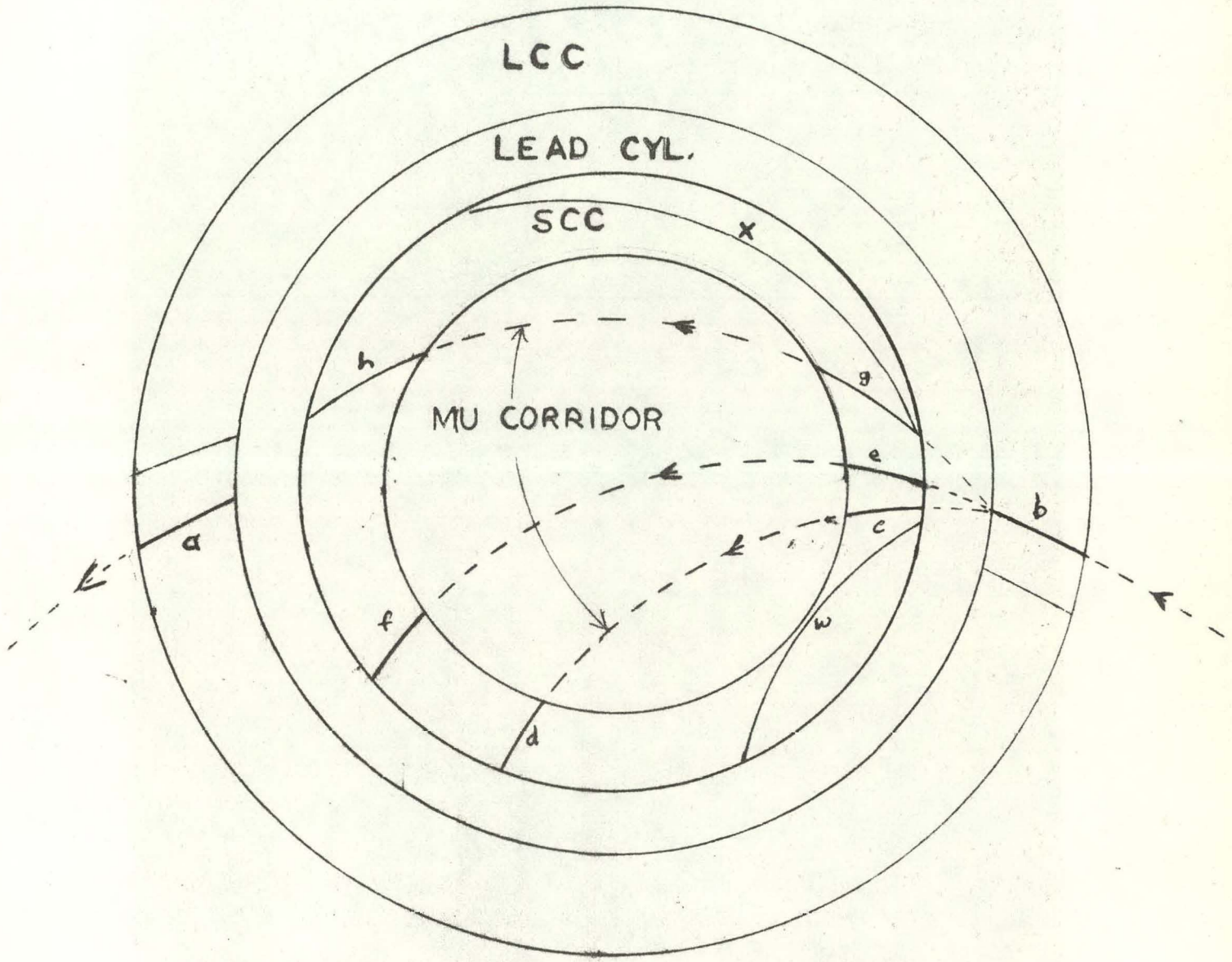

FIG. 12A

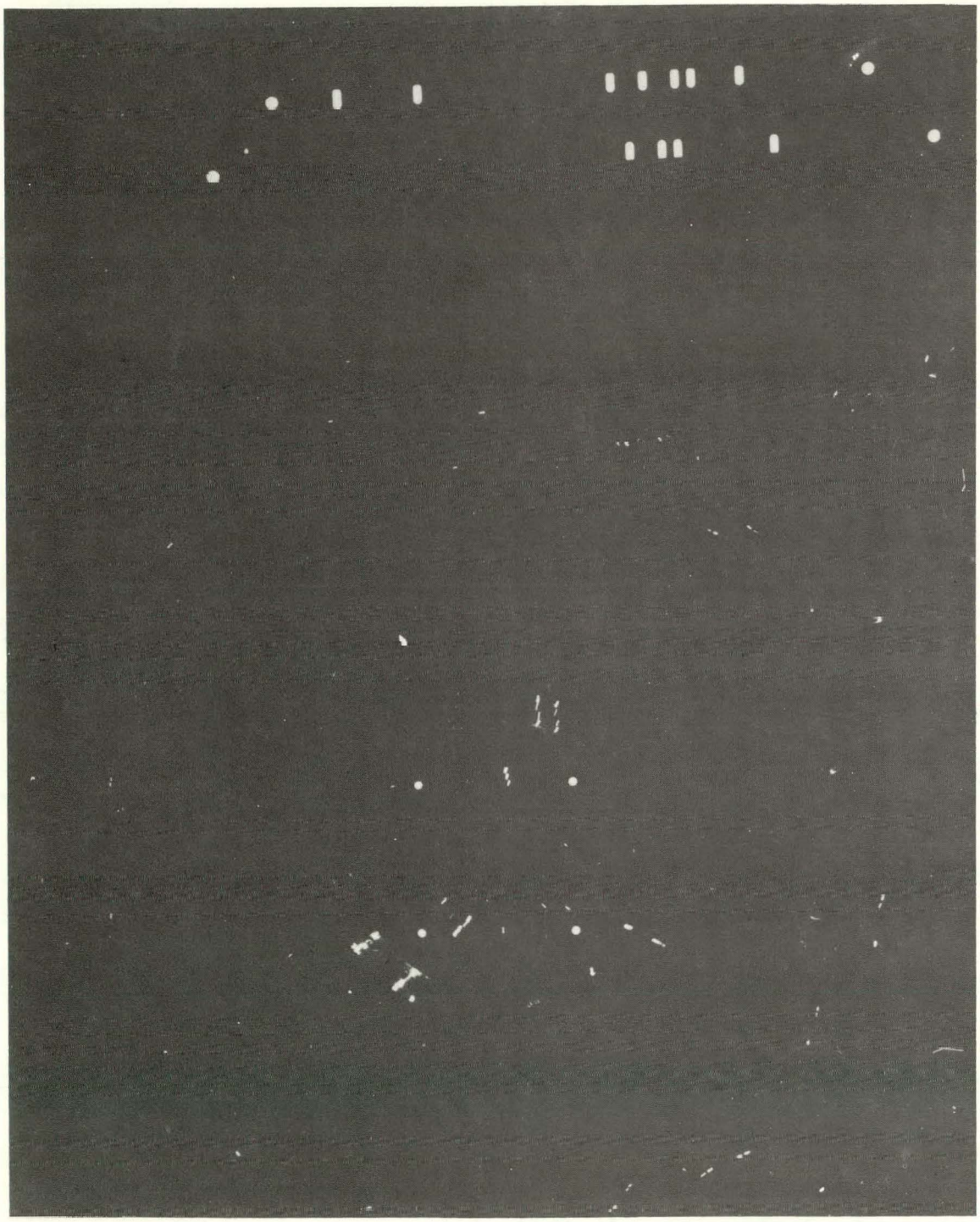

XBB 7010-4520

Fig. 12B

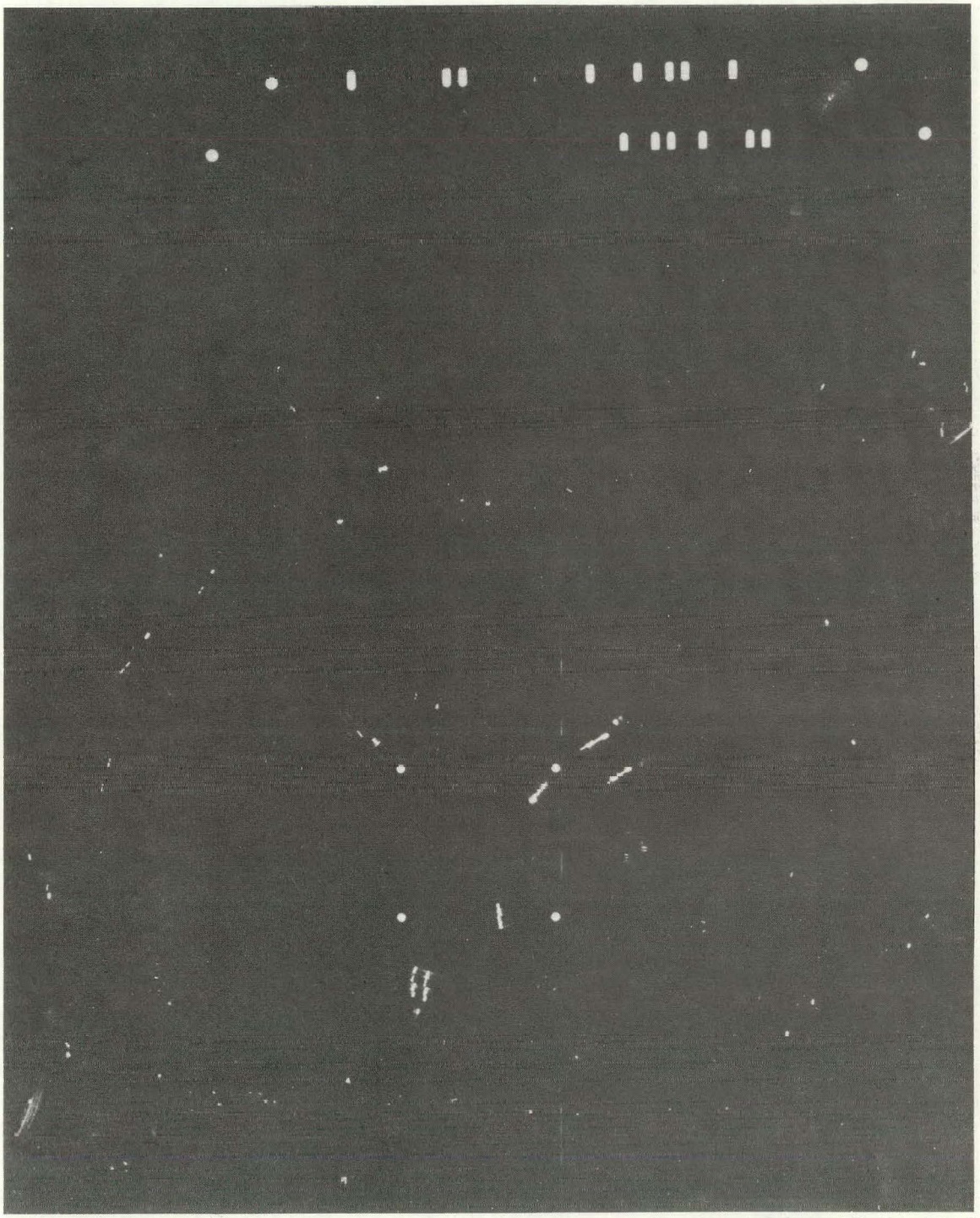

XBB 7010-4521

Fig. 12C

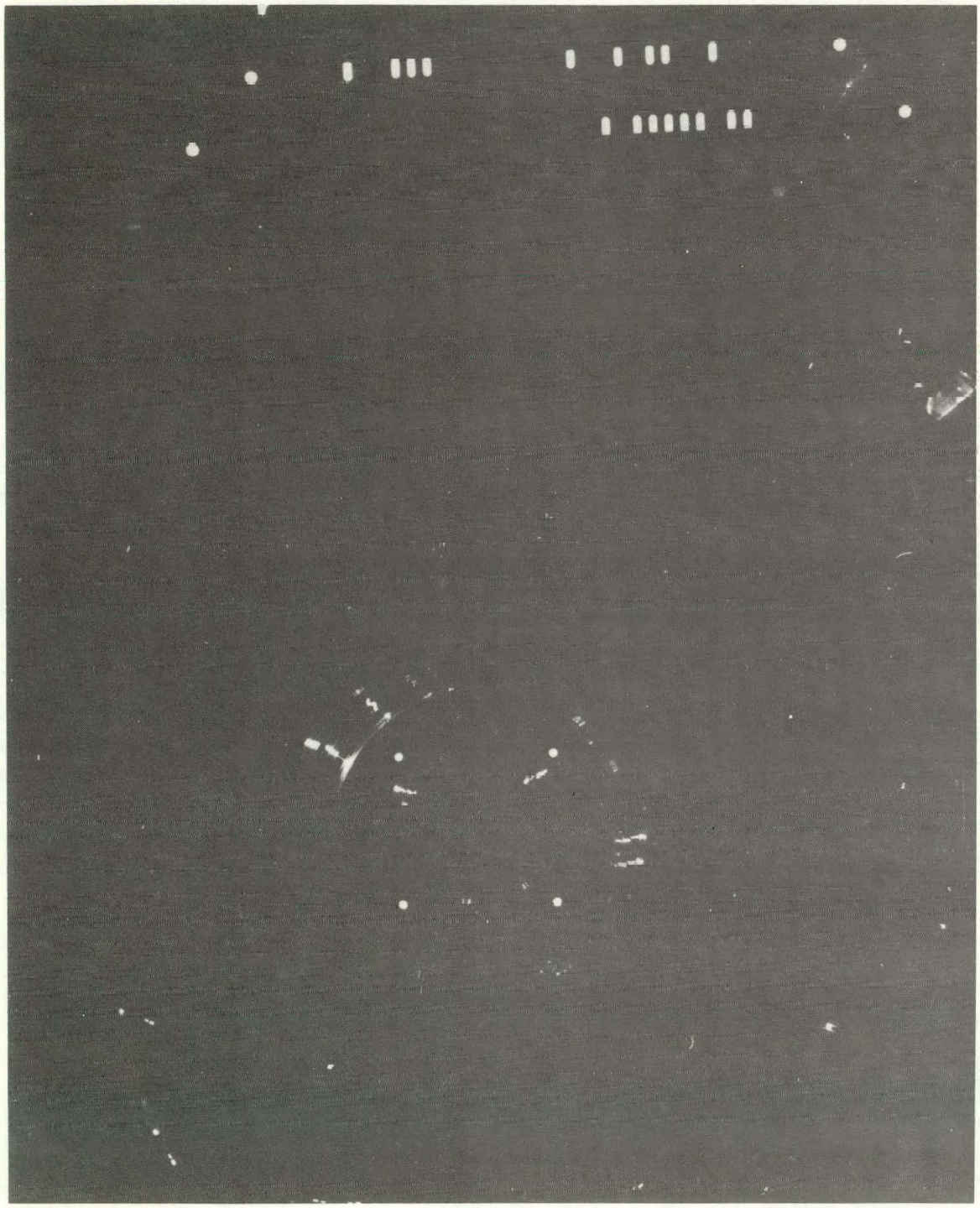

XBB 7010-4522

Fig. 12D

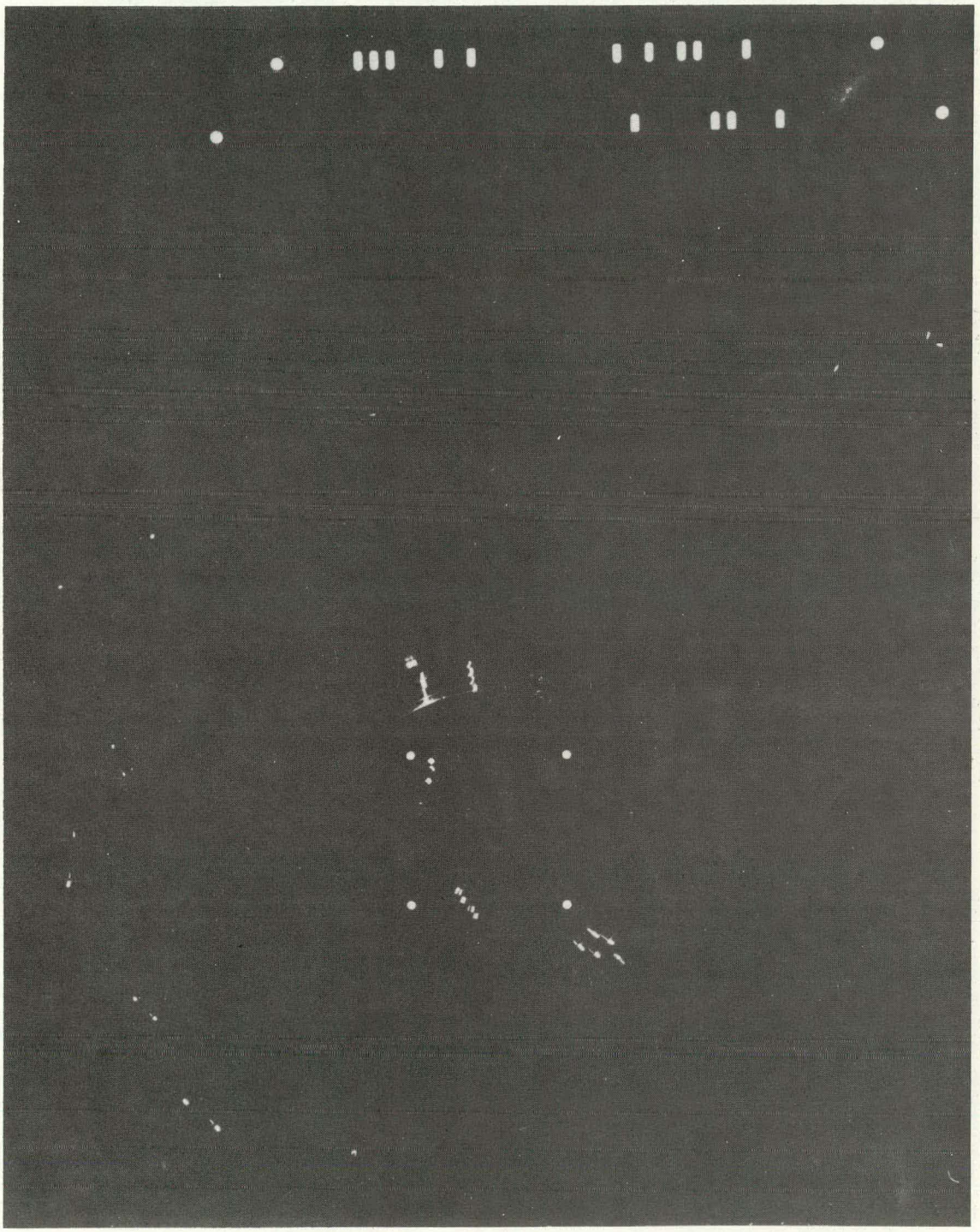

XBB 7010-4523

Fig. 12E

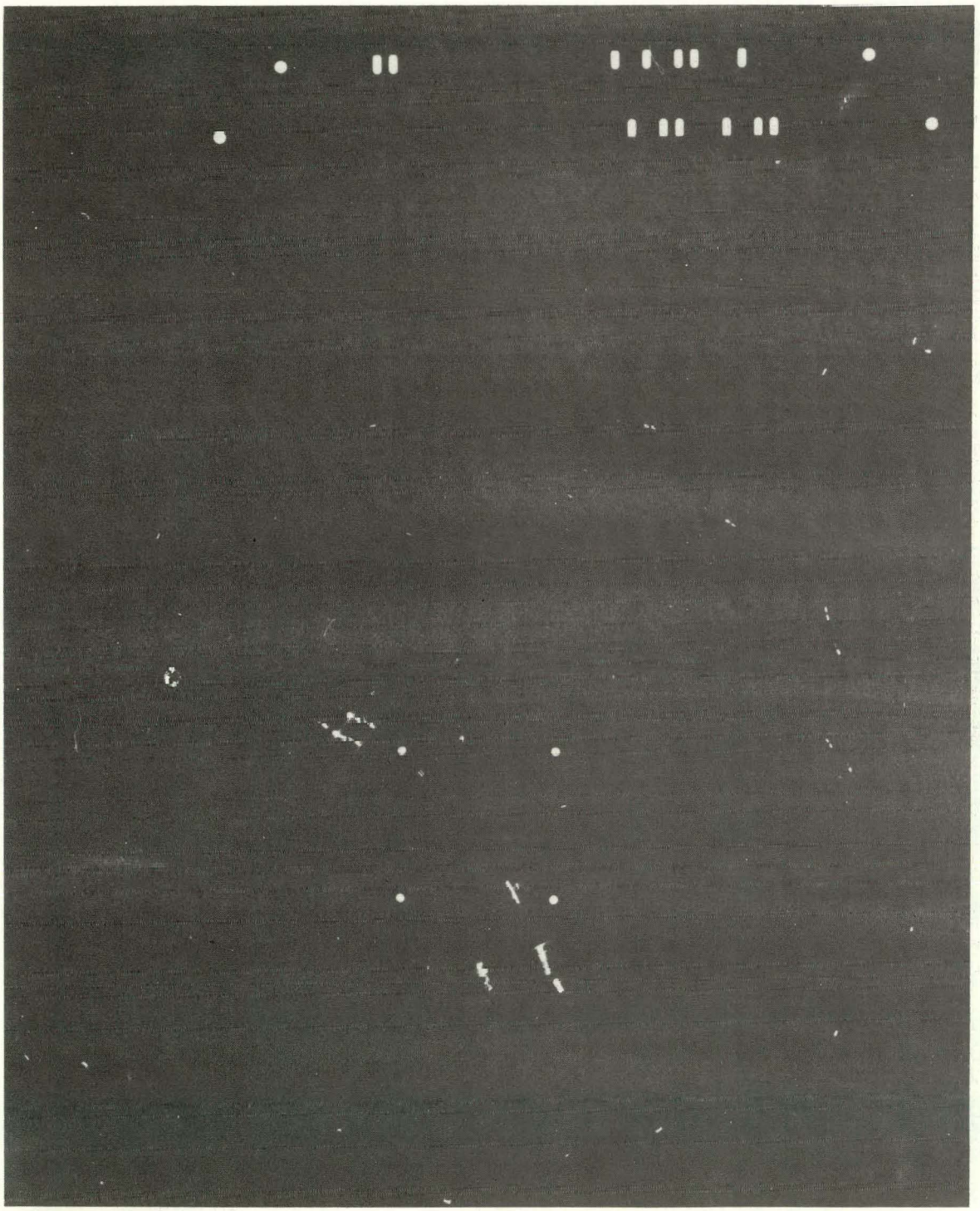

XBB 7010-4524

Fig. 12F

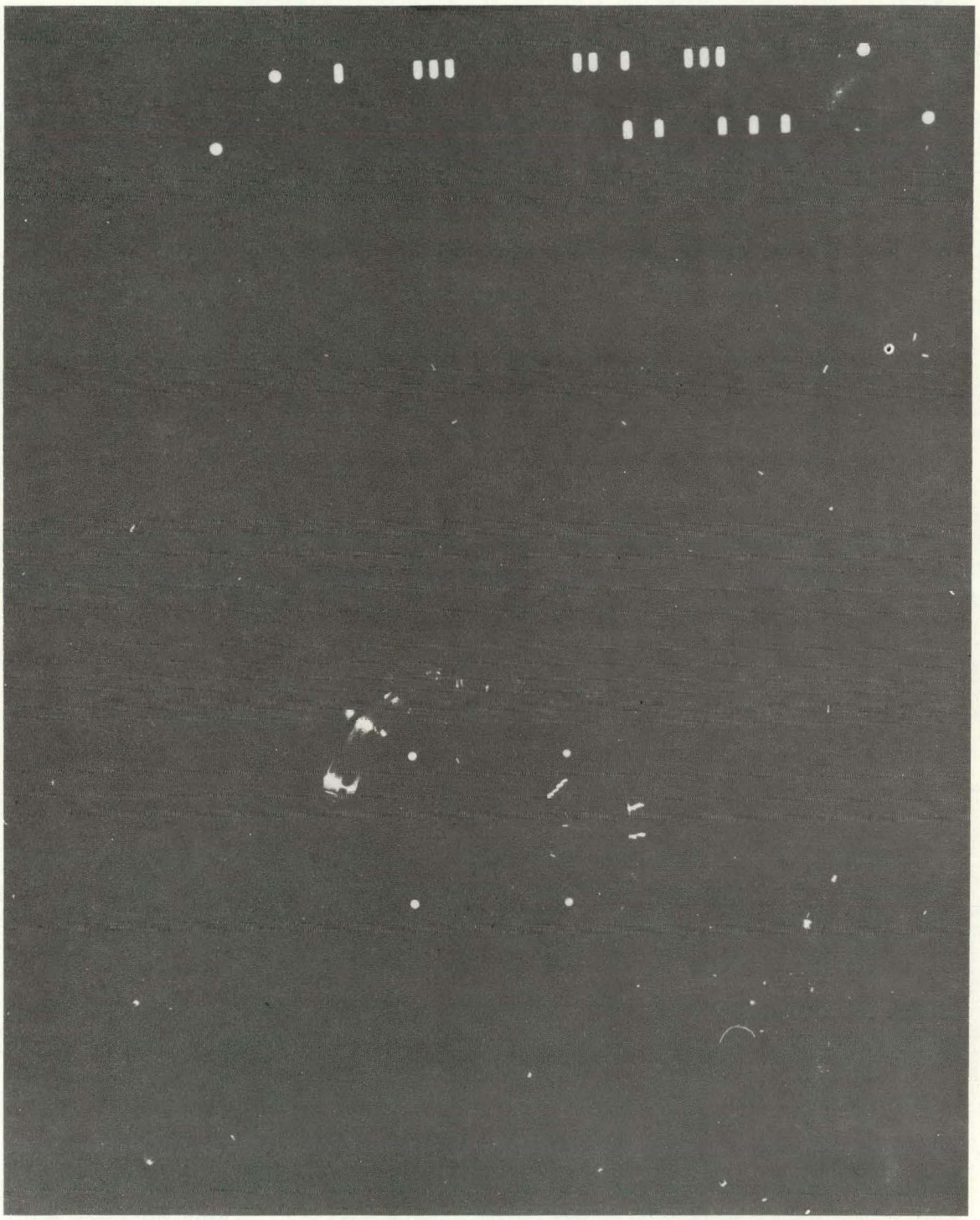

XBB 7010-4525

Fig. 12G

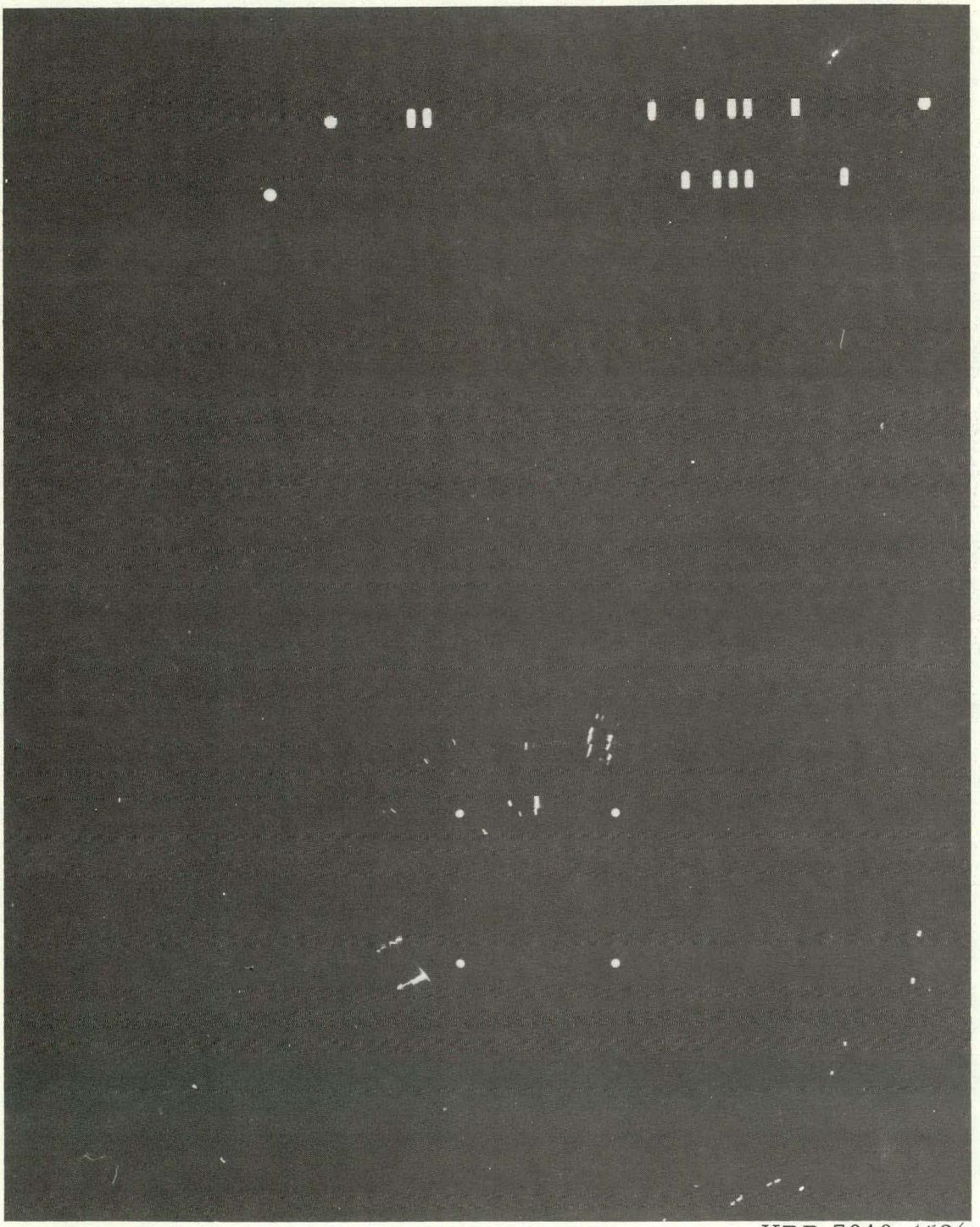

XBB 7010-4526

Fig. 12H

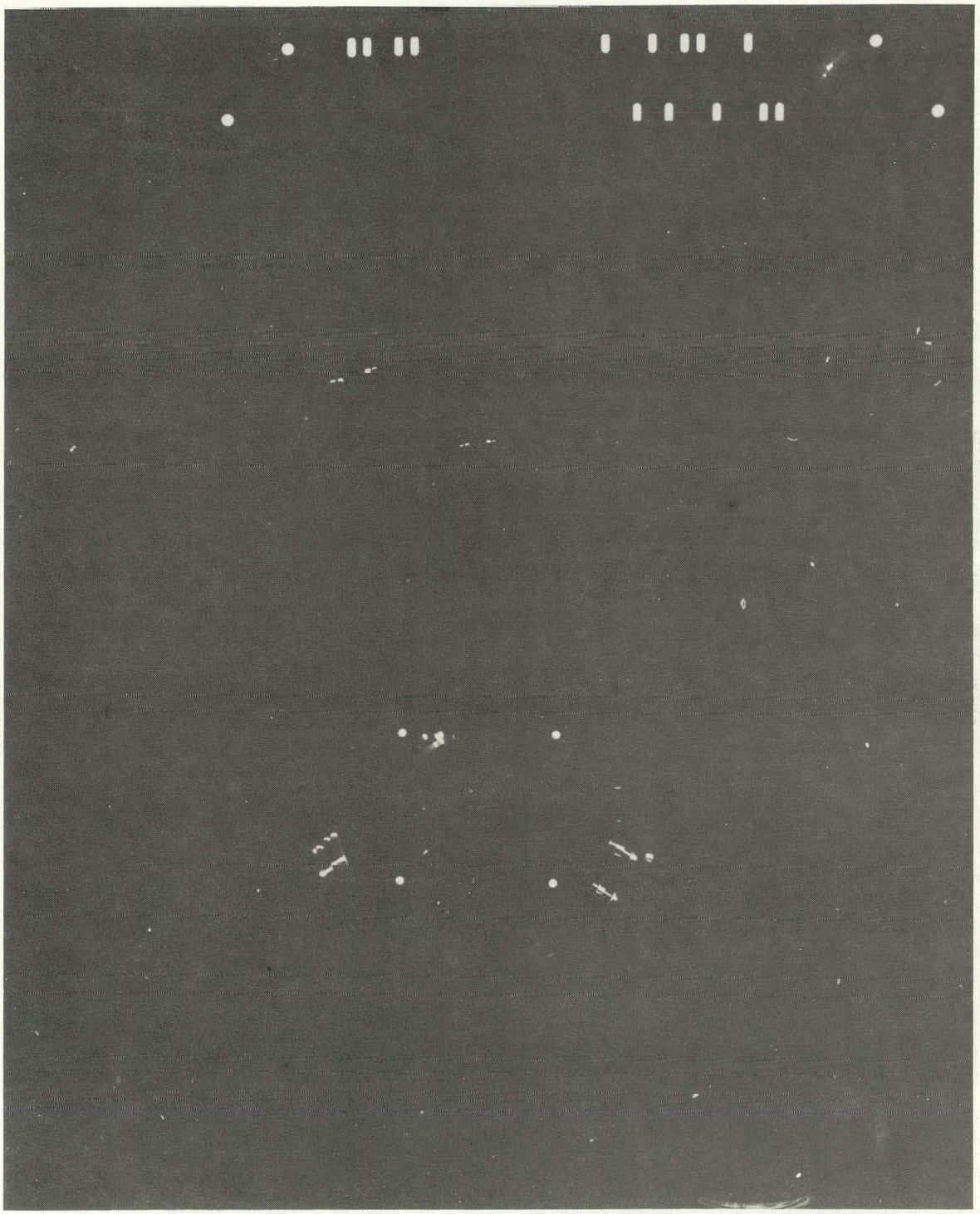

XBB 7010-4527

Fig. 12J

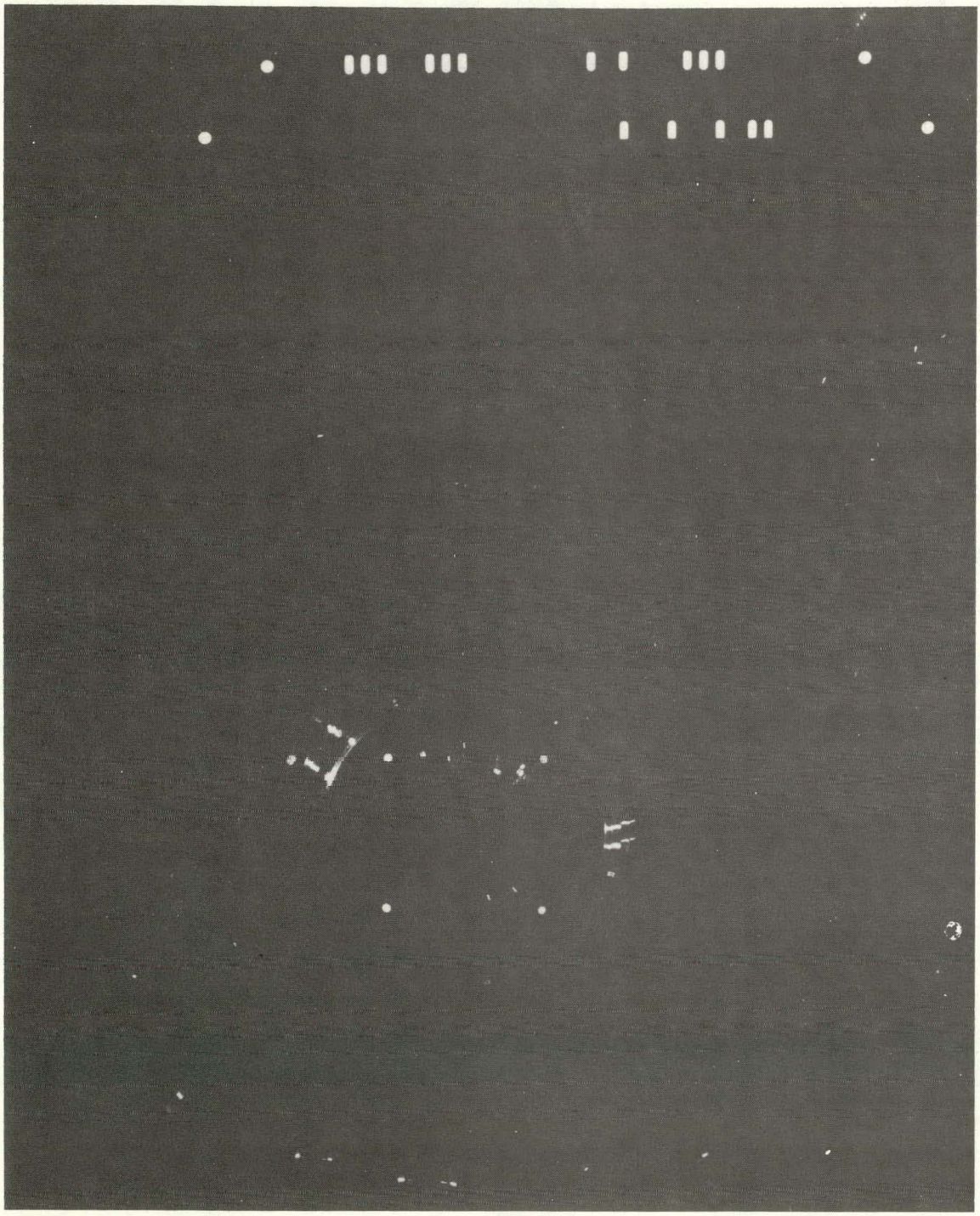

XBB 7010-4528

Fig. 12K

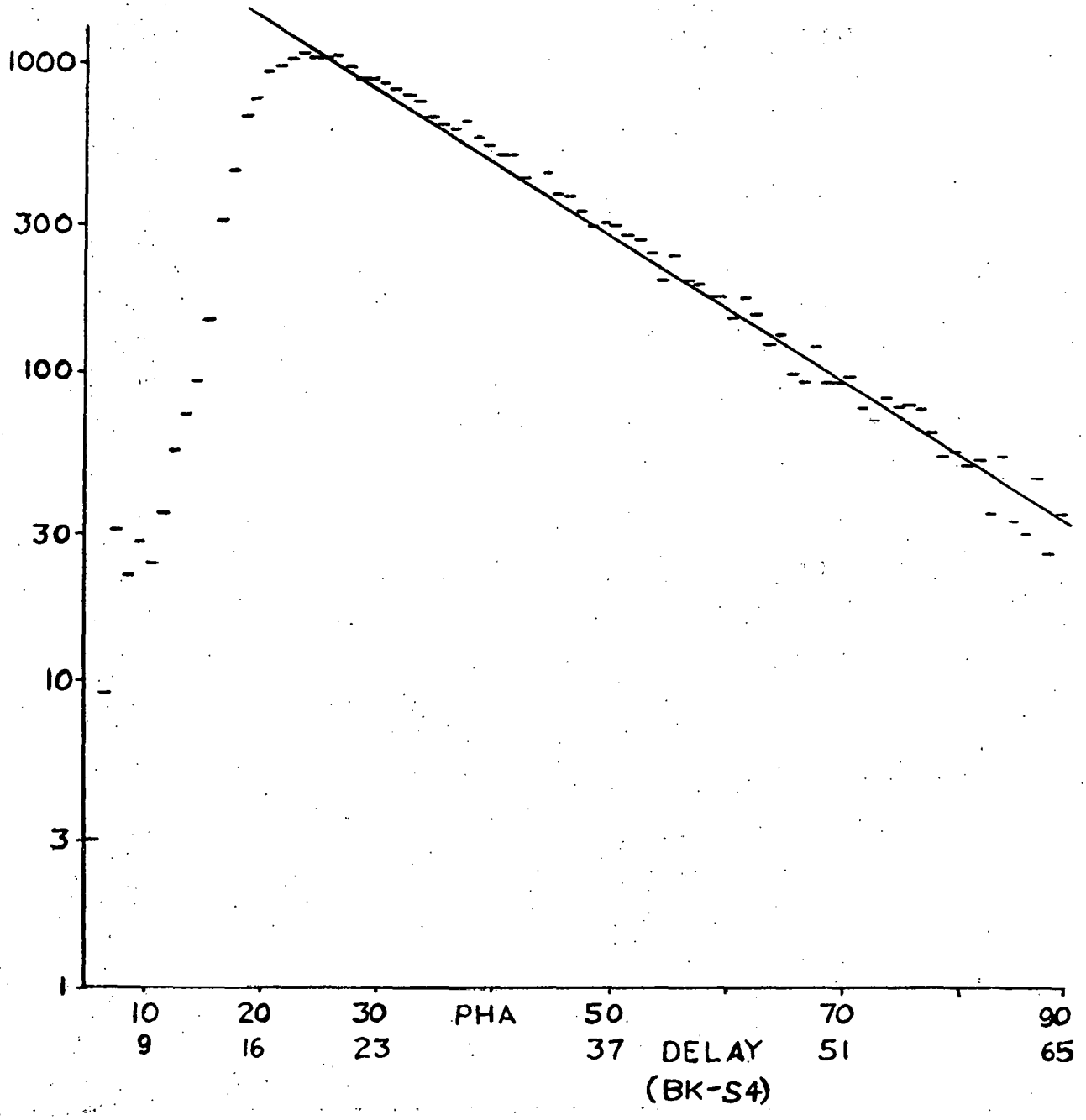
1000
300
100
30
10
3
1
10
9
20
16
30
23
PHA
50
37
DELAY
(BK-S4)
70
51
90
65

FIG. 13A

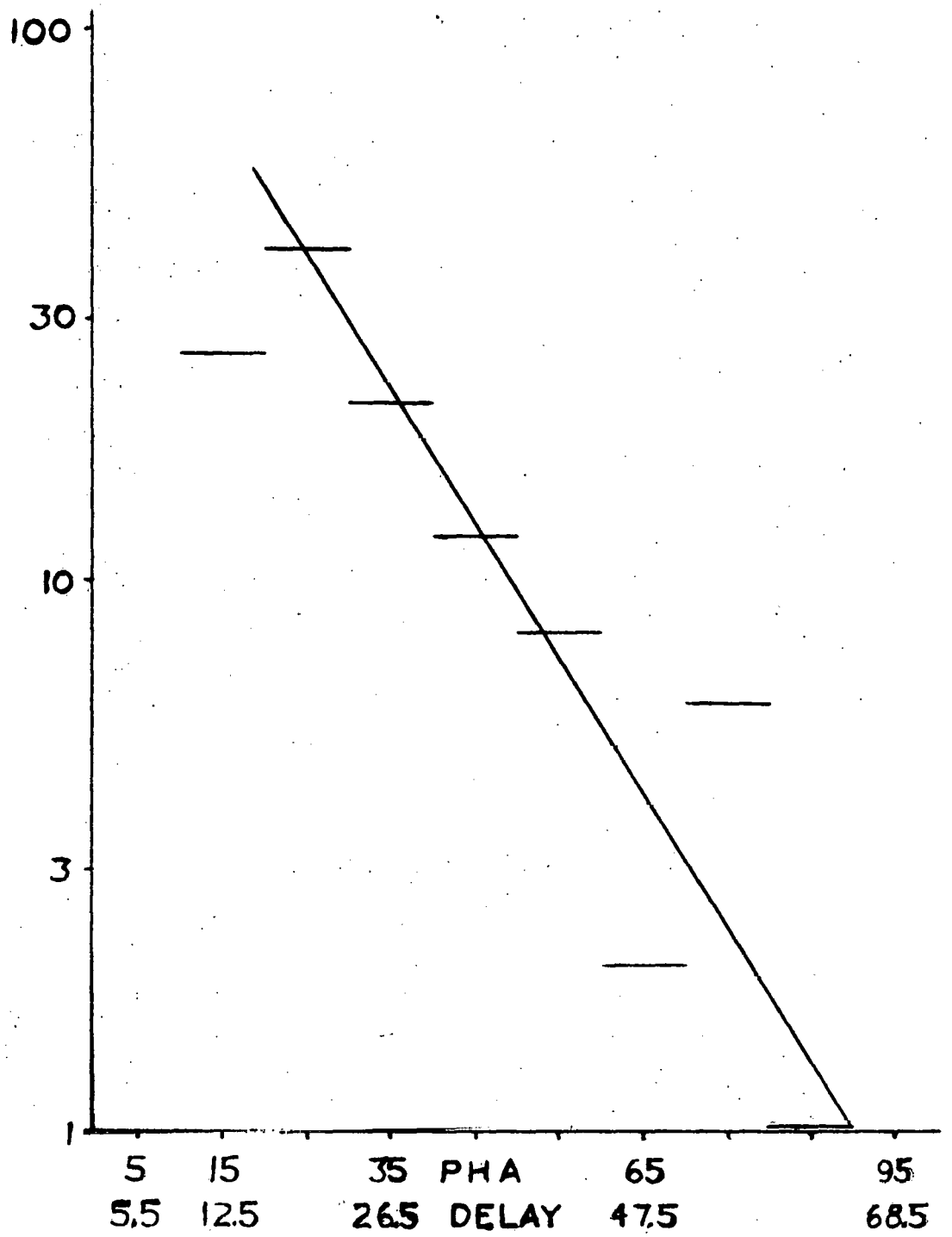

FIG. 13B

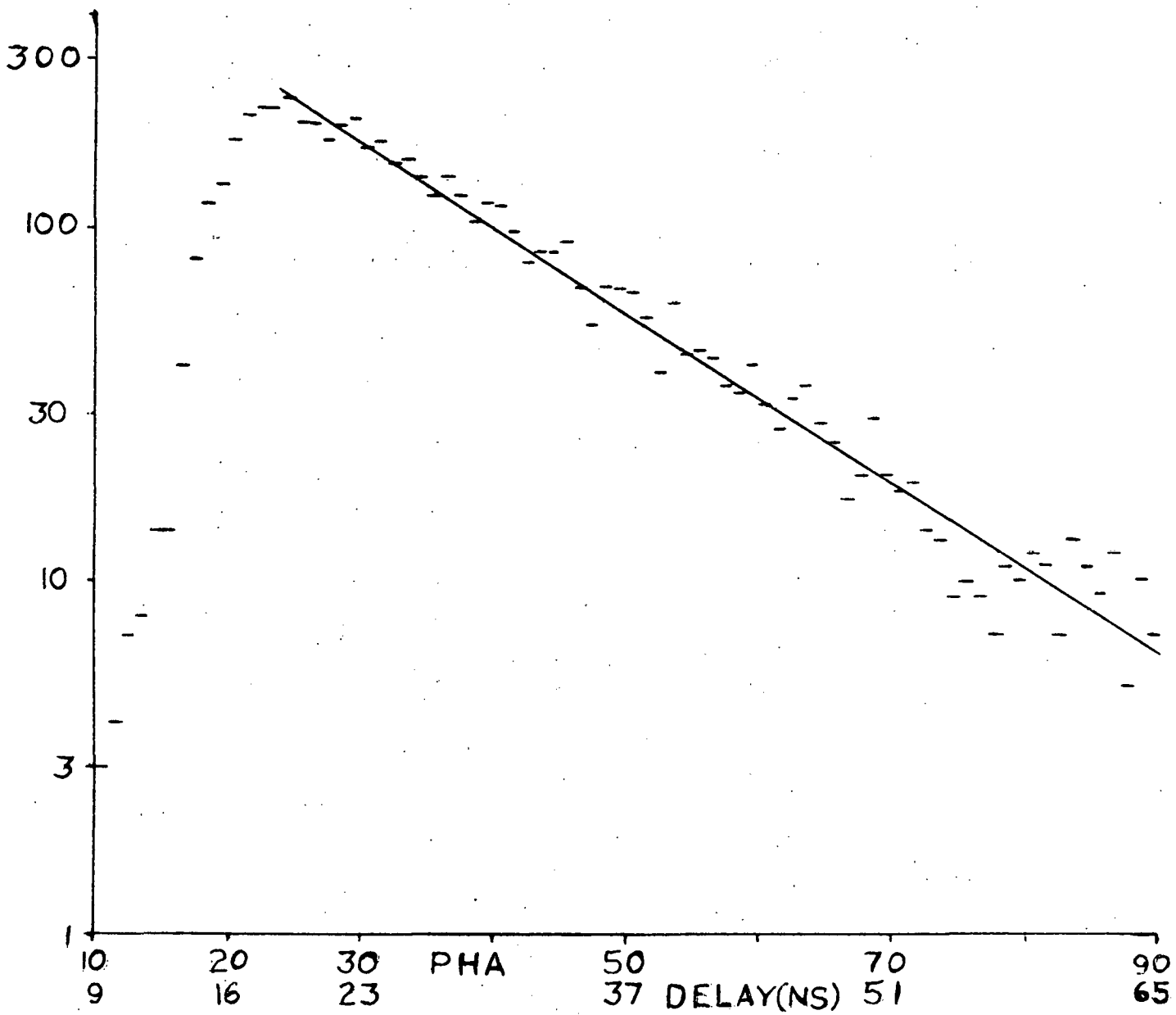

FIG. 13C

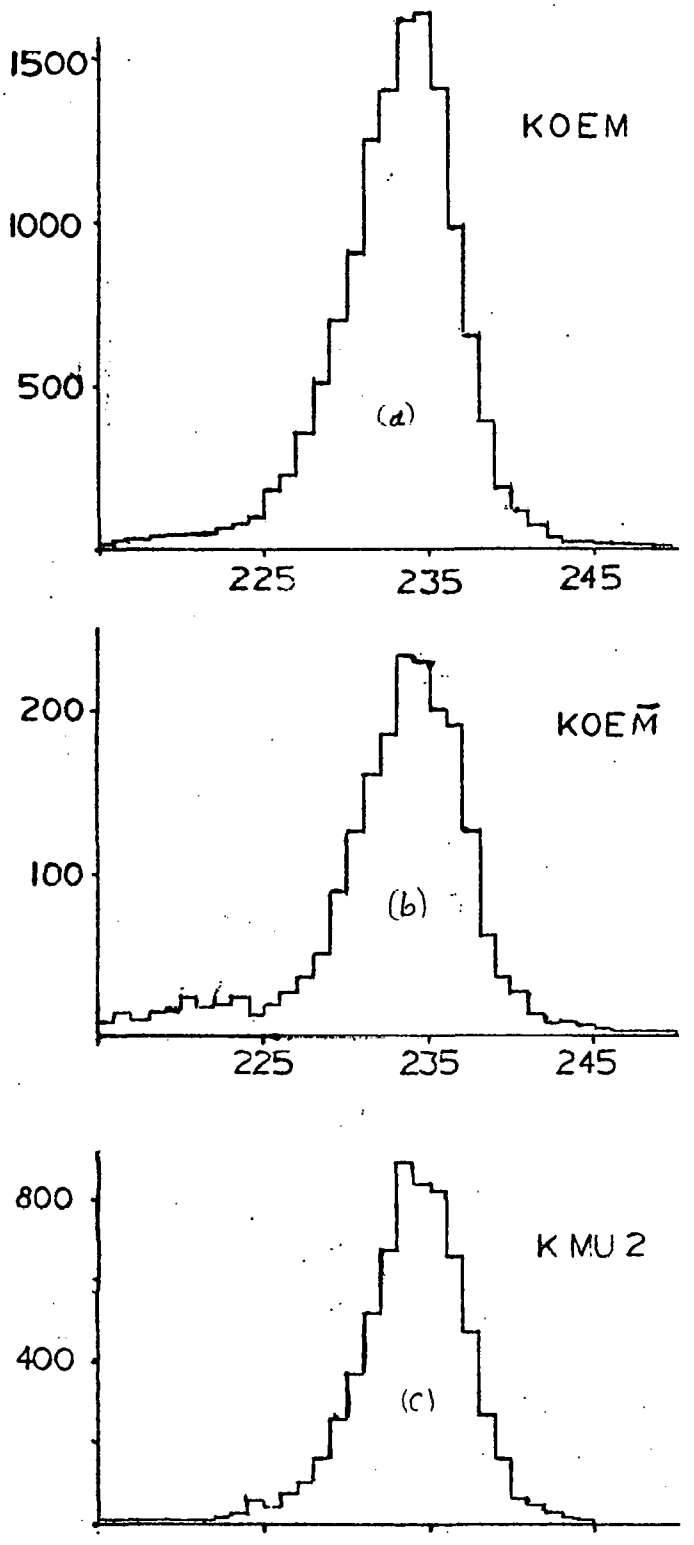

FIG. 14

(a)(b) 72.6 $\times 10^6$ OHM
(c) 89,952 OHM

KOE EVENTS

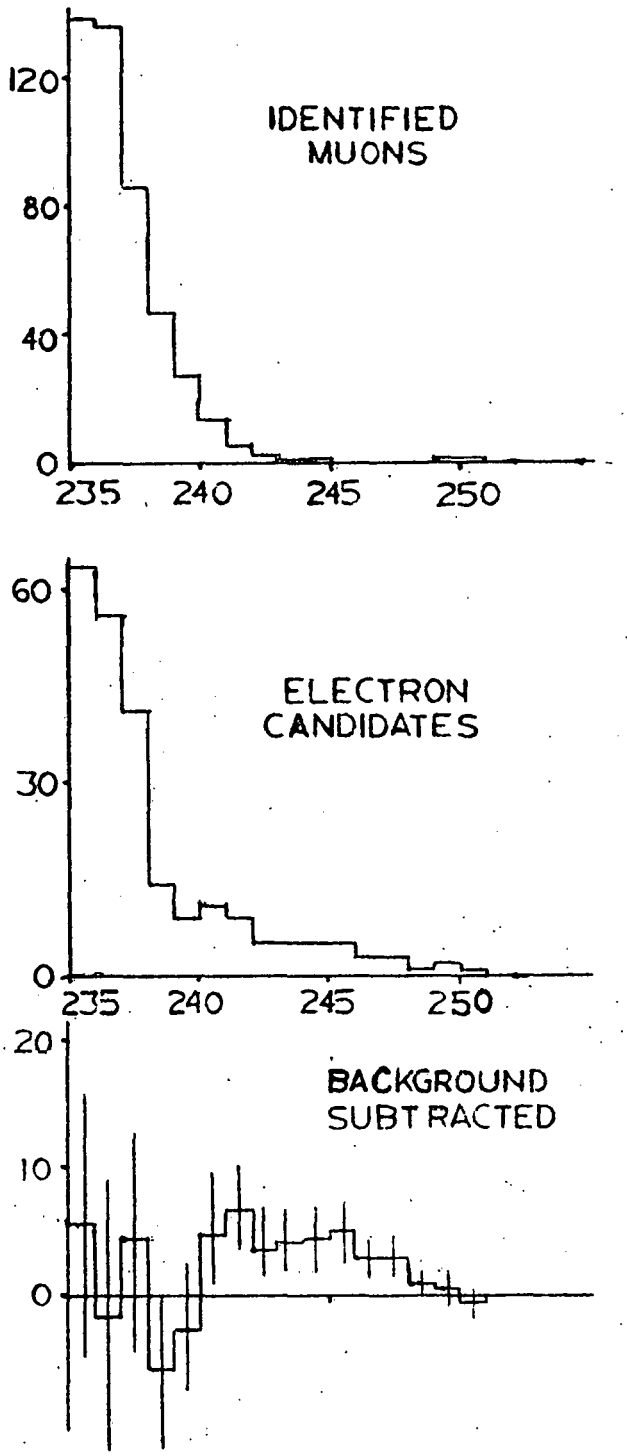

FIG. 15

KOEM EVENTS

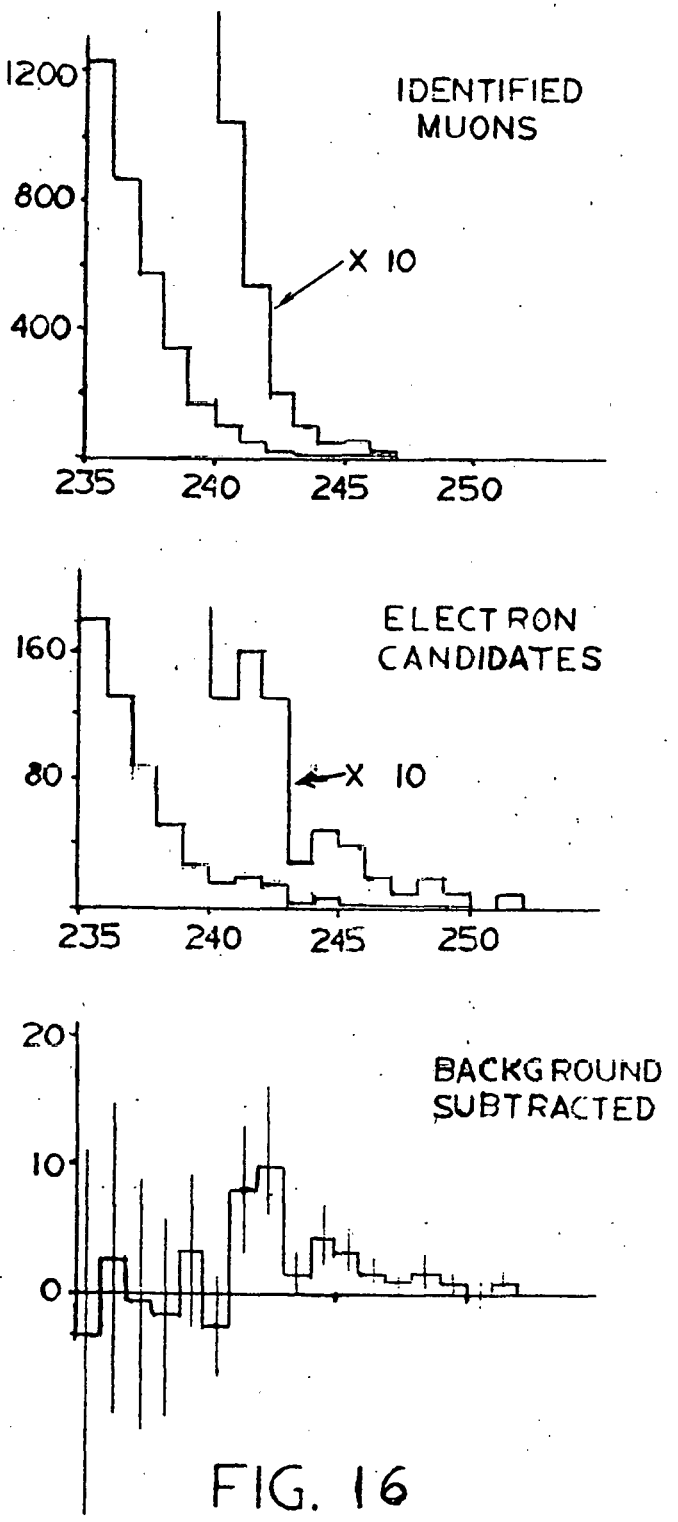

FIG. 16

KE2 SPECTRUM

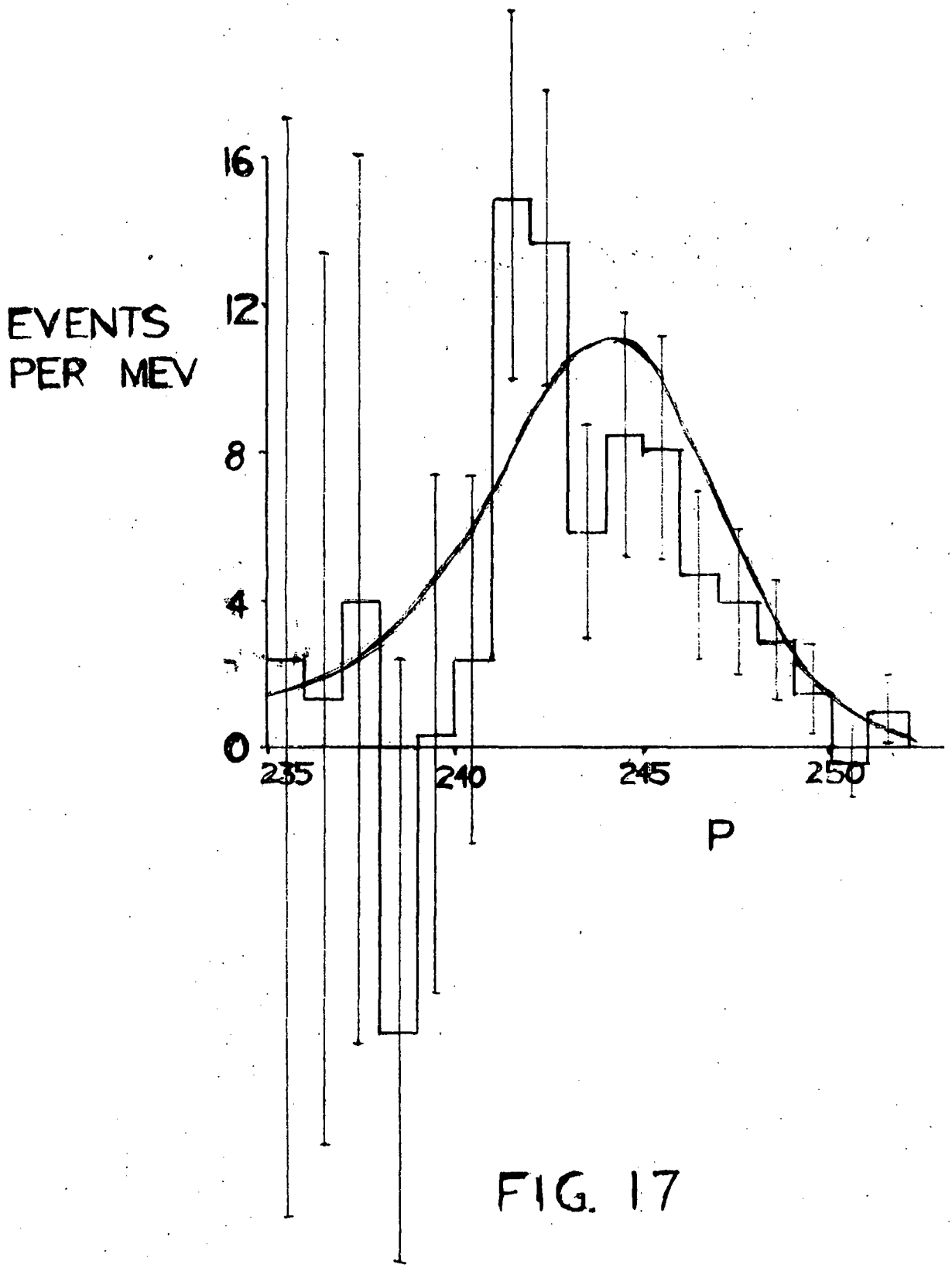

FIG. 17

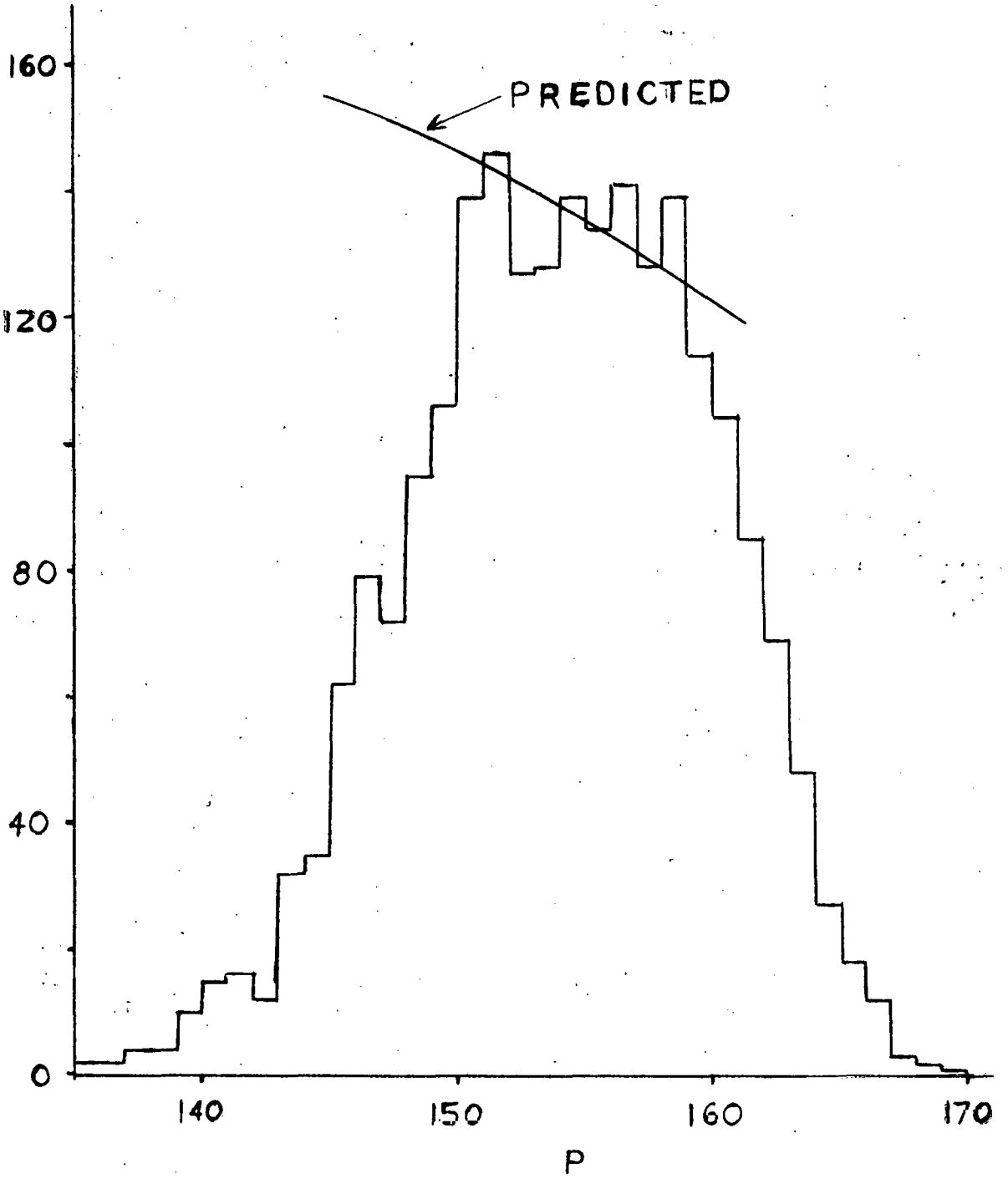

FIG. 18

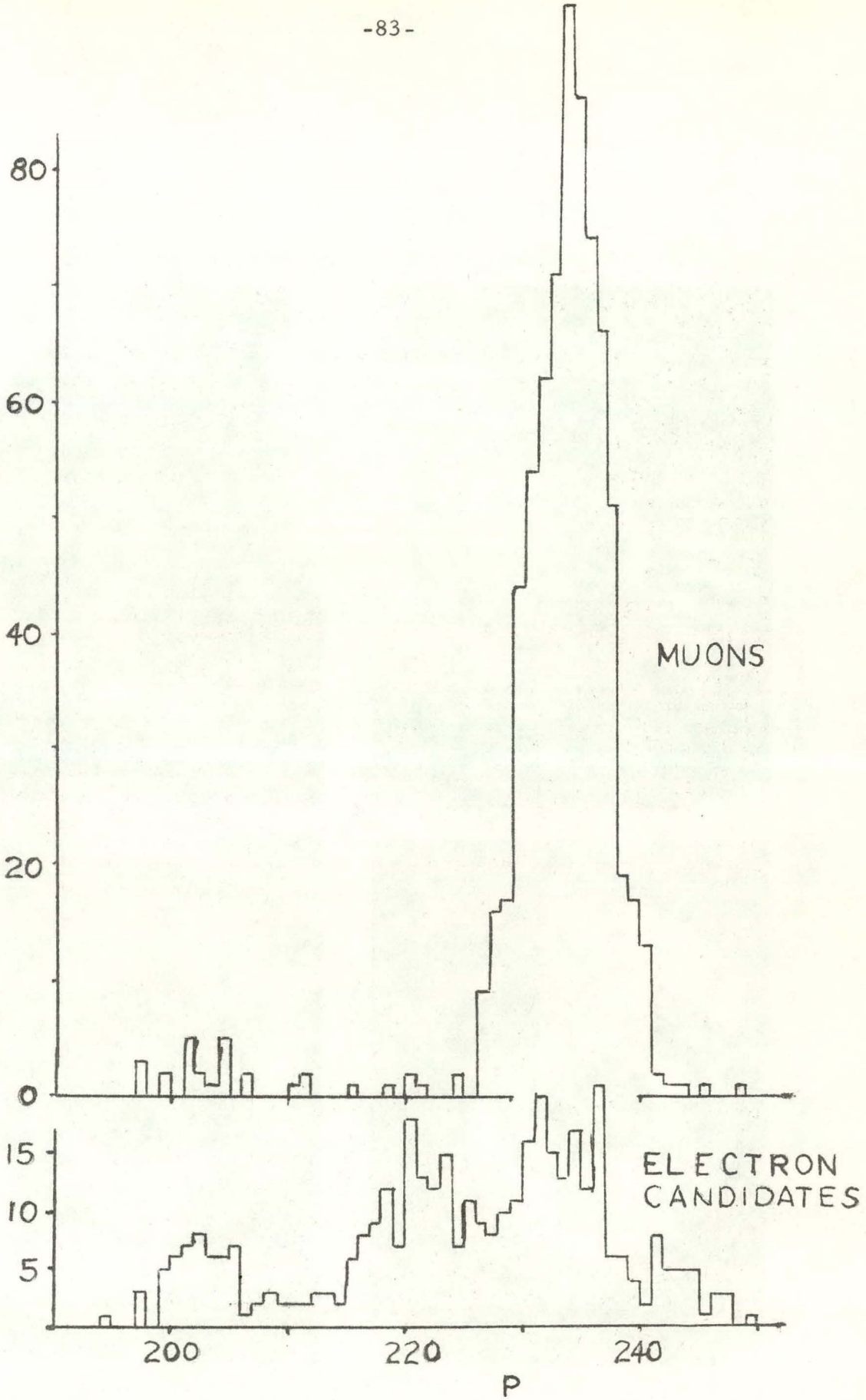

FIG. 19

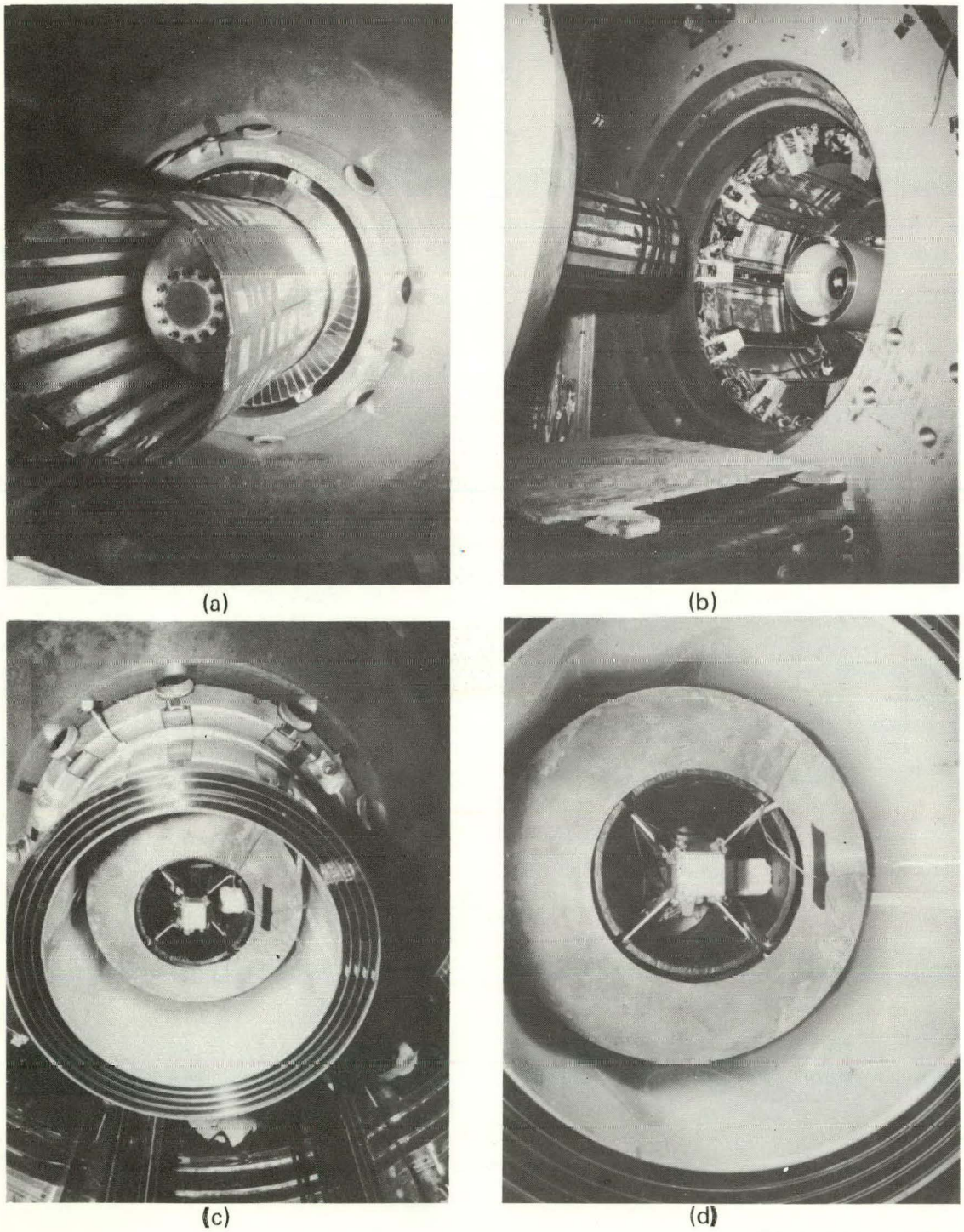

(a) (b) (c) (d)

XBB 7010-4529

Fig. 20

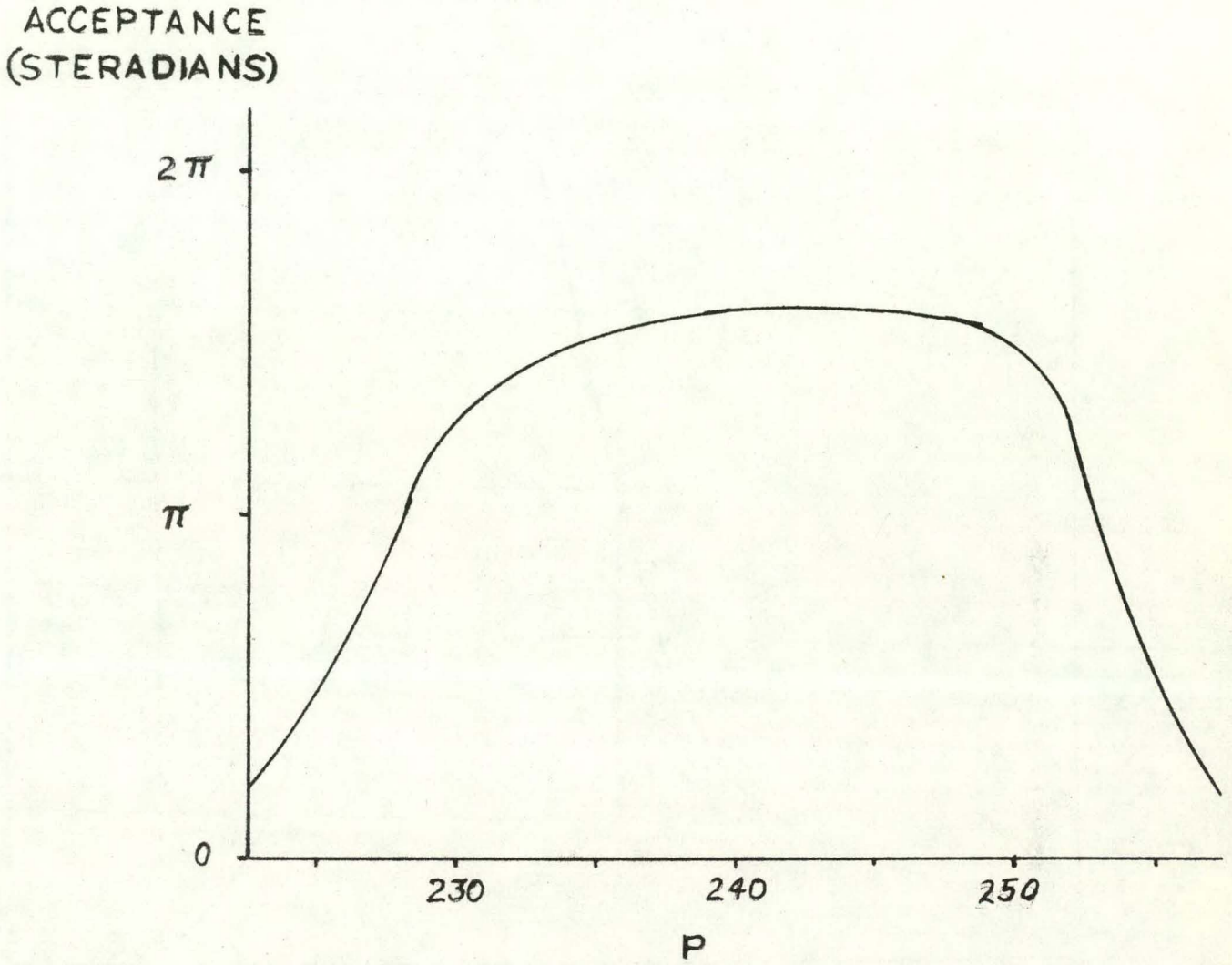

FIG 21

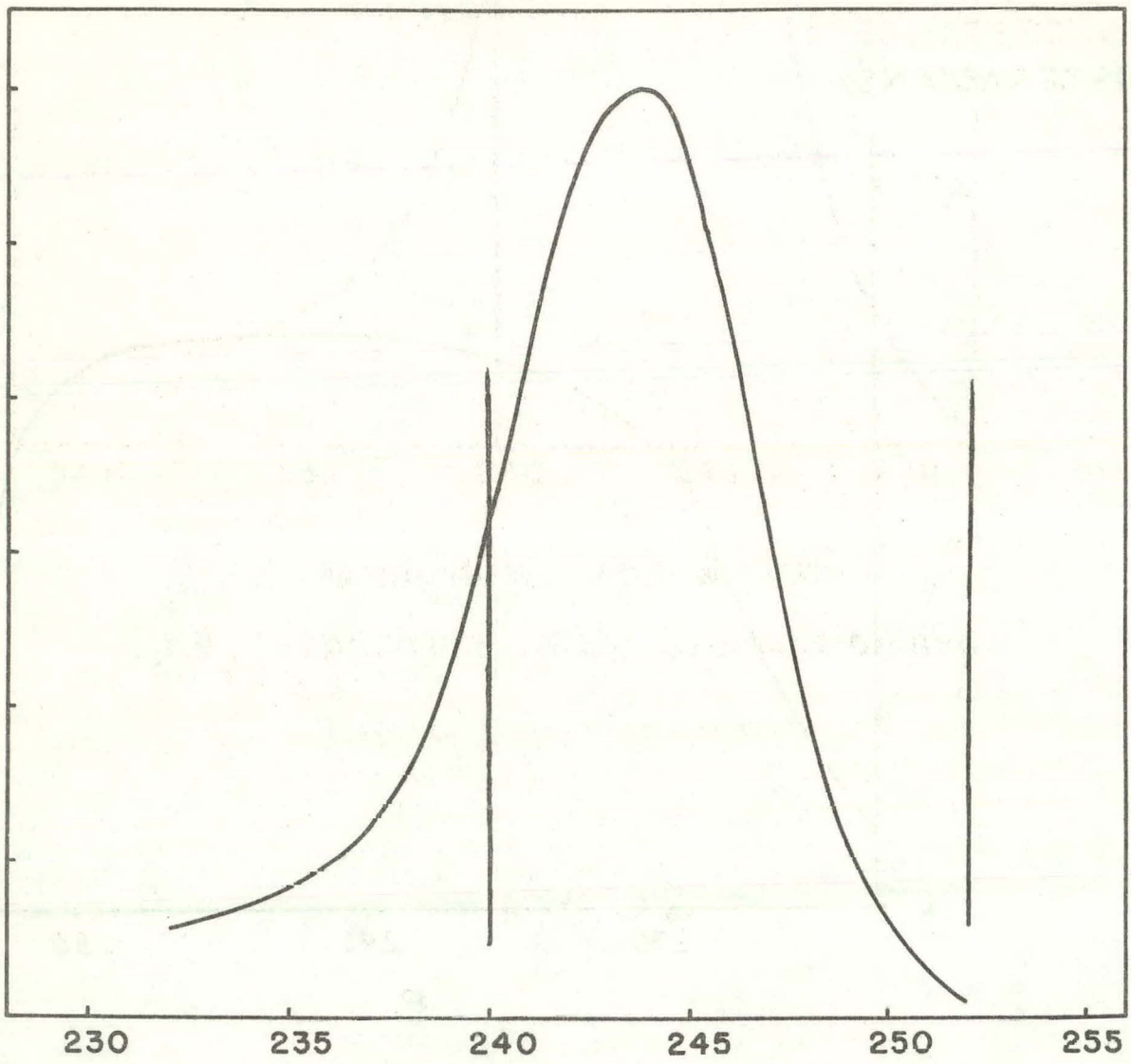

Momentum window and
Ke_2 spectrum with Bremsstrahlung

XBL 708-1780

FIG. 22

TECHNICAL INFORMATION DIVISION
LAWRENCE RADIATION LABORATORY
UNIVERSITY OF CALIFORNIA
BERKELEY, CALIFORNIA 94720